EXPERIMENTAL CHARACTERIZATION OF THE COMPRESSIVE AND SHEAR BEHAVIOR OF SQUARE CELL TITANIUM HONEYCOMB

by

RYAN TYLER PARSONS

B.S., Kansas State University, 2006

A THESIS

submitted in partial fulfillment of the requirements for the degree

MASTER OF SCIENCE

Department of Mechanical and Nuclear Engineering
College of Engineering

KANSAS STATE UNIVERSITY
Manhattan, Kansas

2009

Approved by:

Major Professor

Dr. Kevin Lease

Abstract

The purpose of this study was to experimentally characterize the compressive and shear behavior of square cell titanium honeycomb cores according to the American Society of Testing and Materials Standards C 365-05 and C 273-06. By varying the honeycomb cell size and height as well as the foil thickness, many configurations of titanium honeycomb were manufactured utilizing a laser welding and expansion method. The test matrix consisted of 1080 compression and 1080 shear specimens. The compression specimens were split evenly into stabilized and unstabilized tests, and the shear specimens were split evenly to test three different shear orientations. At the conclusion of the characterization, a comprehensive statistical analysis was performed on the data. It was determined that both the compressive and shear strengths have a strong dependence on the relative density of the honeycomb. The compressive strength was found to be slightly affected by the presence of a stabilizing face sheet, and largely unaffected by specimen core height. The compressive modulus was affected by both the core height and the presence of a face sheet. Shear strength was found to decrease with increasing core height and was influenced by the shear orientation. Additionally, the rate of increase of shear modulus with respect to relative density was proportional to core height. Although no clear trend was observed, orientation did seem to have an effect on shear modulus. The compression and shear behavior of the honeycomb was compared with experimental results of honeycomb from existing publications and found to be consistent.

Note

This thesis follows an alternative format that consists of two journal style manuscripts with an overall introduction and conclusion. Chapter 1 consists of the overall introduction followed by the manuscripts as Chapters 2 and 3 covering the compressive property characterization study and the shear property characterization study, respectively. Concluding remarks from both studies follow in Chapter 4.

Table of Contents

List of Figures

List of Tables

List of Equations

Acknowledgements

This work would not be possible without those whom I have received support throughout my graduated studies.

Dr. Kevin Lease was very instrumental in getting me started in graduate school, keeping me focused throughout, helping me understand the mechanics of materials, and instilling in me, the knowledge to ensure a successful career. Without my co-worker, Liz Frink, this paper would have never been completed on time. I applaud her effort and incredible work ethic.

I am grateful to Benecor Inc. and their chief engineer (Greg Jones) for providing me with the material and insight to complete my research. I would like to thank my committee members for taking interest in my field of study, undergraduate research assistant (Scott Hand) for picking up the slack when I am unable to and providing comic relief when it is most necessary, Jason Selland in the department machine shop for manufacturing custom parts on demand, and the entire Kansas State University Mechanical Engineering Department faculty and staff for creating a great atmosphere for learning.

I am thankful for a very special person (Tiffany Wise) for providing a comfortable and loving environment for me. Without her, this process would have been much more difficult.

I would like to thank my brothers and sister (Josh, Ben, and Sydni Parsons) for supporting me and inspiring me to be a better person every day.

I am indebted to my great grandparents (Lawrence and Francis Parsons) for being hard workers throughout their lives and providing me with the financial support for all of my academics. I am also greatly appreciative of the support I have received from the rest of my grandparents. Thank you for believing in me.

Lastly, and most importantly, I would like to thank my parents (Mark and Lisa Parsons) for raising me, teaching me, providing for me, loving me, and putting up with me. Without them, I would not be the person I am today. To them, I dedicate this thesis.

CHAPTER 1 - Introduction

Honeycomb structures consist of an array of open cells that are constructed from thin sheets of material such as metals, polymers, papers, or natural substances like cork and wood. Metallic honeycomb panel structures have been an important advancement in the aviation and aerospace industry due to their high strength-to-weight ratio. Shear and out-of-plane compression (parallel to the cell walls) are two of the most common loading scenarios that are applied to these structures. Since they are often used in load-bearing, safety critical components it is very important to properly characterize their material properties

This paper focuses on the experimental characterization of the compressive and shear behavior of square cell titanium honeycomb core material. The material was manufactured by Benecor, Inc. (Wichita, KS) and mechanically evaluated by the KSU Mechanical Testing and Evaluation Laboratory (MTEL) (Manhattan, KS). This project was jointly funded by Lockheed Martin and the United States Department of Defense as the first phase of a two phase contract to study the mechanical properties of square cell titanium honeycomb used on the F-35 Joint Strike Fighter (JSF). This phase of the contract involved evaluating the compressive and shear properties of the honeycomb using American Society of Testing and Materials (ASTM) C 365-05 *Standard Test Method for Flatwise Compressive Properties of Sandwich Cores* and C 273-06 *Standard Test Method for Shear Properties of Sandwich Core Materials*, respectively. These two standards describe the testing methods for obtaining the ultimate compressive and shear strengths, as well as compressive and shear moduli. Stabilized and unstabilized compression specimens as well as three different shear orientations were evaluated. The second phase of the contract will involve the characterization of beam flexure and tensile behavior (at ambient and non-ambient conditions), and will also be performed at MTEL.

CHAPTER 2 – Compressive Behavior of Square Cell Titanium Honeycomb*

Introduction

Honeycomb cores are commonly used in applications where one of their primary functions is to carry compressive load in the out-of-plane direction, parallel to the walls that form the honeycomb cells. In this direction the individual cell walls are in compression rather than bending so the structure is very stiff and capable of sustaining high loads. Honeycomb cores are typically used in sandwich applications where they are bonded between two thin, stiff face sheets to increase their resistance to bending. Their high resistance to bending and compression, coupled with their low density, makes composite sandwich structures ideal for aircraft and aerospace applications.

This paper discusses the results of a rather large experimental program aimed at the characterization of compressive properties of a laser welded square cell titanium honeycomb product, following ASTM C365-05 *Standard Test Method for Flatwise Compressive Properties of Sandwich Cores* [1.1]. In this study a total of 1080 specimens were tested – half of the specimens were unstabilized (no face sheets applied) while the other half were stabilized (face sheet adhesively bonded to one side). Multiple parameters were evaluated by varying the specimen cell size (l), core height (h), and foil thickness (t) (or cell wall thickness), which are shown in Figure 1.1. Each combination of cell size and foil thickness defines a "configuration", which includes three core heights and two "specimen types" (stabilized or unstabilized). This paper will also discuss the results of this program and a comprehensive statistical analysis of the data.

*This chapter is in the format of a manuscript intended for submittal to the *Journal of Experimental Mechanics*. Authors on this paper consist of Ryan Parsons, Elizabeth Frink, Kevin Lease, Suzanne Dubnicka, and Greg Jones.

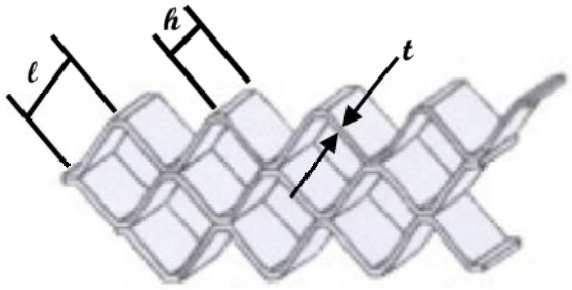

Figure 1.1: Illustration of square cell honeycomb with foil thickness (t), cell size (l), and core height (h) [1.2]

Material and Manufacturing Processes

The manufacturing process for the square cell titanium honeycomb in this paper involves a proprietary laser welding technique developed by Benecor Inc. (Wichita, KS). Benecor receives the ASTM certified Ti 3A1-2.5 2B annealed coil foil (nominal properties: σ_y = 910 MPa, E = 100 GPa, ν = 0.3) on oil free rolls of a specified foil thickness and width.

The manufacturing of the honeycomb core product involves several steps and begins with producing a "block" of foil material. Sheets are first cut from the titanium foil so that the length of foil removed from the roll is equal to the desired height (along the out-of-plane axis) of the block. The width of the roll of foil is the limiting factor for how wide a block can be. Two sheets are stacked, and then, using the proprietary laser welding process, a weld along the height of the sheets is made at predetermined intervals along the width of the sheets. The interval spacing determines the cell size of the honeycomb, and Benecor has developed a program that determines the laser welding interval for a given cell size. Each weld interval actually consists of several weld "spots", with a predetermined spacing, along the core height. Although the details of this spacing are proprietary, an example image is shown in Appendix A. At the end of each length of foil, the welding head returns to its start position for the next layer. Layer after layer of foil is welded until the required number of layers has been applied. At this point, the stacked and welded sheets are referred to as a block.

Each block is sliced into sections of the desired core height using a variety of metal cutting methods (e.g. EDM, water-jet), depending on the specified tolerance. The sliced section is then expanded (perpendicular to the surface of the sheets) to its full width and

length (expansion direction) and is then referred to as a "blanket". Images of representative weld "nodes" can be seen in Appendix A. A weld node is the portion of foil length that is mated to another foil length creating a very strong point at the corner of each square cell. Final trim is performed (using an appropriate cutting method for the desired tolerance) to yield the final length and width requested by the customer.

In preparing the test specimens for this study, each blanket was hand-marked using templates made specifically to the ASTM test standard specimen size requirements. Test specimens were then cut using a water cooled, diamond-encrusted (abrasive) blade. The unstabilized test specimens were cut to final ASTM dimensions of 76.2 x 76.2 mm (3" x 3"). Initially, the stabilized specimens were cut using a 152.4 x 228.6 mm template, then adhesively bonded to a 0.79 mm aluminum stabilizing plate and finally cut into six 76.2 x 76.2 mm specimens. Later in the study, stabilized specimens were first cut into 76.2 x 76.2 mm samples and then bonded to a thin stabilizing plate. This change in procedure occurred due to a concern that cutting the larger stabilizing sheets after bonding may cause the adhesive bond to fail during the cutting process. There was no discernible difference in compressive properties demonstrated between these two bonding and cutting scenarios. Once prepared, all ASTM required dimensions were measured and recorded for each specimen.

In an attempt to evaluate differences between specimens from different blocks of material, a "group" of five "batches" of six specimens (cut from the same blanket) were tested for each foil thickness, cell size, core height, and specimen type combination in this study. In each configuration the first batches came from the same block, and similarly for the remaining batches.

Test Matrix

The test matrix consisted of six configurations, including both stabilized and unstabilized (from now on referred to as "bare") specimens. Each configuration corresponds to a relative density, defined as:

$$\bar{\rho} = \frac{2t}{l}. \tag{1.1}$$

In this study, foil thicknesses of 0.025, 0.038, and 0.051 mm, and cell sizes of 2.743 and 3.175 mm were used. Each configuration had three core heights: 6.35, 12.7, and 15.875 mm, and for each core height there were five batches of six specimens for a total of 90 bare and 90 stabilized specimens per configuration.

The six different configurations were designated by the letters B, A, E, D, G, and Q (in order of increasing relative density). The configuration letter designations were chosen by the manufacturer to correspond to their existing labeling system. Table 1.1 shows the test matrix, which specifies the combination of foil thickness and cell size corresponding to each configuration. To distinguish between the two specimen types, the stabilized specimens were labeled "SC" and the unstabilized (bare) specimens were labeled "UC". The core heights were assigned the numbers 1 thru 3 which corresponded to the three heights: 6.35, 12.7, and 15.875 mm, respectively. The batches were identified by the numbers 01 thru 05 and the individual specimens were identified by the numbers 01 thru 06. Each specimen was given an eight digit identification code, which consisted of the configuration letter, the core height number, the specimen type designation, the batch number, and the individual specimen number. An example specimen identification code can be seen in Figure 1.2. The entire test matrix, summarized in Table 1.1, consisted of 540 bare compression tests and 540 stabilized compression tests.

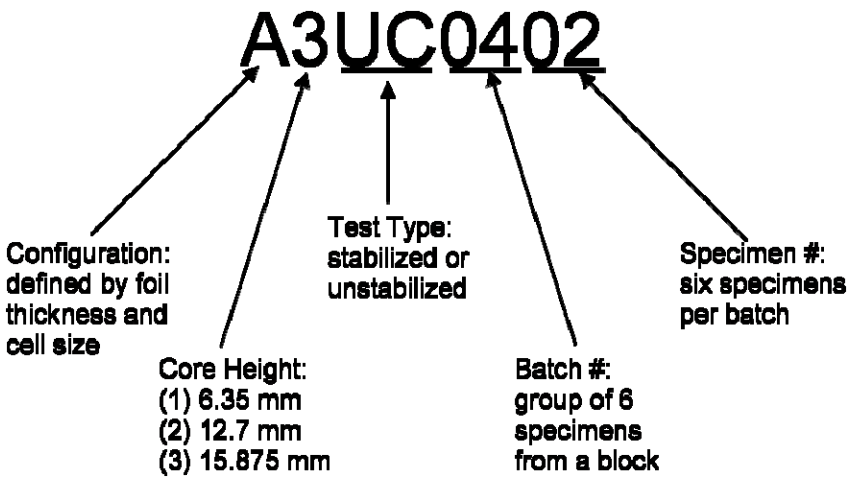

Figure 1.2: Example specimen identification code. This code is for the second unstabilized specimen from configuration A, batch 04 with a 15.875 mm core height.

Table 1.1: Test matrix with relation to identification code conventions

Configuration	Foil Thickness [mm]	Cell Size [mm]	Relative Density	Core Height [mm] (designation)	# of Specimens (5 batches per thickness)	
					UC	SC
B	0.025	3.175	0.016	6.35 (1)	30	30
				12.7 (2)	30	30
				15.875 (3)	30	30
A	0.025	2.743	0.019	6.35 (1)	30	30
				12.7 (2)	30	30
				15.875 (3)	30	30
E	0.038	3.175	0.024	6.35 (1)	30	30
				12.7 (2)	30	30
				15.875 (3)	30	30
D	0.038	2.743	0.028	6.35 (1)	30	30
				12.7 (2)	30	30
				15.875 (3)	30	30
G	0.051	3.175	0.032	6.35 (1)	30	30
				12.7 (2)	30	30
				15.875 (3)	30	30
Q	0.051	2.743	0.037	6.35 (1)	30	30
				12.7 (2)	30	30
				15.875 (3)	30	30
			Total # of Tests		1080	

Experimental Procedure

The experimental procedure followed ASTM standard C 365-05, which provides the standard test method for obtaining the flatwise compressive strength and modulus for bare specimens, which have no facings, or for stabilized specimens, which have a thin facing applied to one or both sides. Both bare and single facing, stabilized compression tests will be discussed in this paper. The ASTM standard test procedure was followed with two exceptions. First, the standard recommends a preload of 45 N be applied to the specimens, but it was found that a heavier preload of 90-135 N was necessary to properly seat the specimen with the spherical head platen. Second, the standard states that the displacement sensor should be zeroed after the preload is applied and before the testing begins. With the test control and data acquisition system used in this project, it was more convenient to skip this zeroing step and zero the resulting data during data analysis.

All tests were performed at room conditions on a 245 kN Instron 8502 servo-hydraulic test machine using a commercially available compression platen set, seen in Figure 1.3, incorporating a spherical seat platen on the top and a fixed bottom platen with an integrated LVDT (instead of the internal ram displacement sensor) as per ASTM requirements. The LVDT made contact with the upper platen via a rod inserted through a central hole in the lower platen and a hole drilled in the center of the face sheet of stabilized specimens.

Figure 1.3: Image of compression test fixture

The tests were performed at a constant displacement rate, which varied for each configuration (0.09 mm/min for the smallest relative density to 0.15 mm/min for the largest relative density), to ensure that the samples failed within the ASTM required time frame of three to six minutes. All analog signal data (force, crosshead displacement, and

integrated LVDT) were recorded three times per second using a customized LabVIEW Virtual Instrument (VI). Along with the external signals, the VI was also programmed to automatically record the specimen number and the run-time as well as user inputs of specimen length, width, and height. The test date and test conditions (temperature and relative humidity) were also entered by the user and recorded. All signals and user inputs were saved to a spreadsheet file for documentation and data analysis.

Specimens were received from the industrial sponsor with accompanying final measurements of the specimen length, width, and thickness recorded to three significant figures. Each specimen was loaded individually, resting on the center of the lower platen between the two compression platens to a pre-load of 90-135 N. The test rate was set at the appropriate value and the displacement control test proceeded until the specimen had exhibited uniform compression failure. Each resulting output file contained the data for the six separate specimens in a given batch.

Data Analysis

After the tests were completed, data analysis was performed on each raw data output file using a custom Microsoft Excel VBA macro. This analysis involved the calculation of compressive strength and modulus as per ASTM C365-05 guidelines. The compressive strength, σ_c (referred to in the standard as the ultimate flatwise compressive strength, F_z^{fcu}), for each test is defined as

$$\sigma_c = \frac{P_{\max}}{A}, \tag{1.2}$$

where P_{max} is the ultimate force prior to failure, and A is the cross-sectional area (nominally 75.6 x 75.6 mm) [1.1]. The compressive modulus is defined as the slope of the linear region of the stress-strain curve. The suggested method, from ASTM C365-05, for determining the compressive modulus involves a two-point slope calculation over the linear region of the force-displacement curve shown in Figure 1.4. For this study, a regression slope method was chosen over the two-point slope method due to the potential for increased accuracy and ease of implementation. The standard also gives the option of

calculating the 2% deflection stress; however, this property was not calculated in this study because only a fraction of the compression tests were carried out to a deflection that corresponded to 2% strain.

From the raw data file, the macro separated the six tests of a given batch into six tabs in Excel and graphed the force-displacement and the stress-strain curve for each test. Instantaneous stress was obtained by dividing the force data by the specimen cross-sectional area (nominally 5806 mm^2) and instantaneous strain was calculated by dividing the corresponding displacement by the original specimen core height. An interactive prompt allowed the user to view the force-displacement curves and define an appropriate linear region for the batch. A linear regression was performed on each test to determine the chord slope (illustrated between points C and D in Figure 1.4), and the resulting compressive modulus of each specimen. Seating of the specimen during testing causes a toe region to be present in the force-displacement curve. This region was removed from each curve using the chord slope, as described in ASTM C365-05. After calculation of compressive strength and modulus was completed for each test in a group, means and standard deviations were calculated for each batch of 6 and the group of 30. A more thorough statistical analysis was performed on all of the configurations after the completion of all data analysis and will be discussed in a later section of this paper.

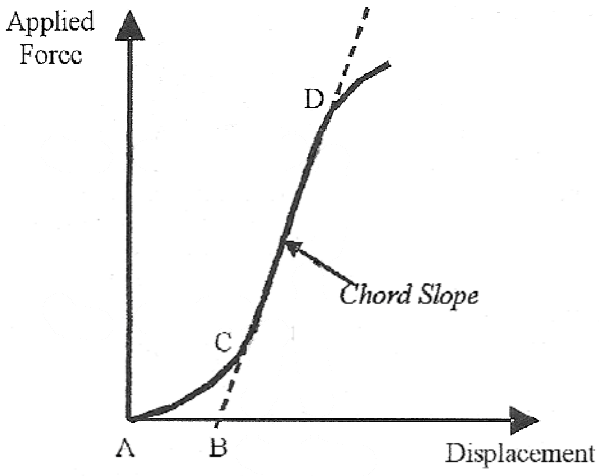

Figure 1.4: Illustration of force-displacement curve before manipulation showing the chord slope and the toe region [1.1]

Results and Discussion

Representative stress-strain curves for stabilized and bare compression specimens for each configuration are shown in Figure 1.5. The nature of the core failures varied slightly across the test matrix and between stabilized and bare tests, but for the most part the appearances of the stress-strain curves were fairly consistent.

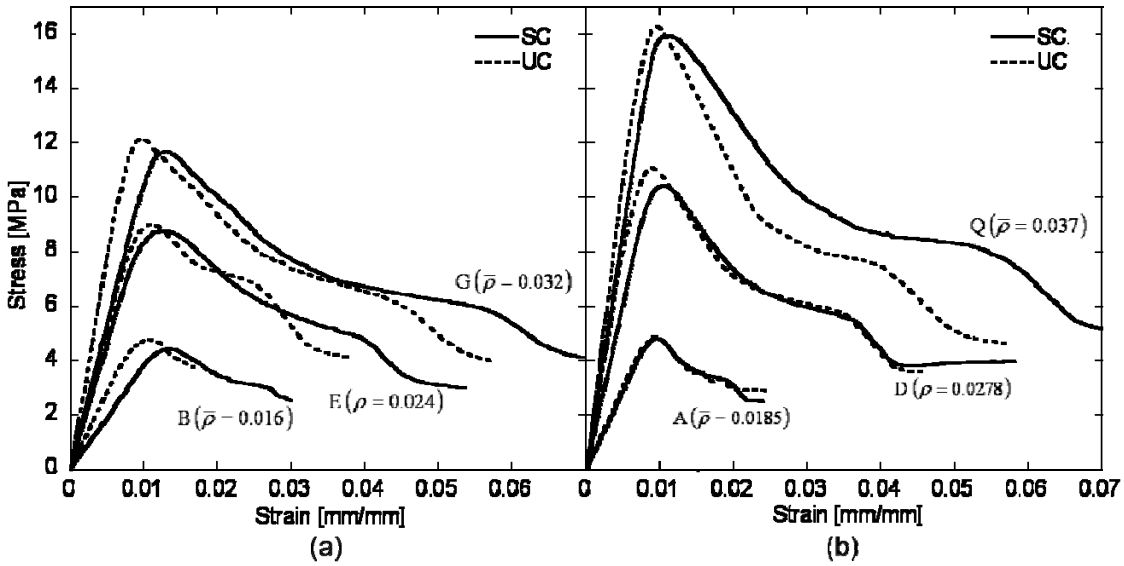

Figure 1.5: Stress-strain response of the stabilized and bare tests for configurations (a) B, E, and G and (b) A, D, and Q

All of the curves began with a stable linear elastic region. Following this linear elastic region, the curves then reached a peak compressive force at which point the specimen began to fail. The maximum force represents the transition of the cell walls to instability. As soon as the peak is reached, the cell walls begin to fail as the specimen begins to structurally soften and continue to soften until the test is ended. It was also observed that the specimen parameters (foil thickness, cell size and cell height) had little effect on the strain at failure. Approximately 90% of all of the specimens had a peak force between 1% and 2% strain with the majority of the bare compression specimens exhibiting a peak force at approximately 1% strain. The overall appearance of the compression stress-strain curve obtained in this study is similar to that reported by Côté *et al*. for 304 stabilized and bare stainless steel square cell honeycomb (five different relative densities and two different aspect ratios (h/l); slotted and then welded; σ_y = 210 MPa) and 3003

grade aluminum hexagonal cell honeycomb (three relative densities and one aspect ratio; formed and then welded; σ_y = 210 MPa) [1.3].

After the initial failure and structural softening, the curves appear to have a secondary step-down that is more pronounced in the specimens with larger relative densities, as can be seen by configurations D, G, and Q in Figure 1.5. This is possibly due to the increased resistance to cell wall buckling at higher relative densities, which delays the formation of additional folds in the cell walls after the initial fold. Once these stiffer cell walls begin to form additional folds, the stored energy is quickly released and the loads drop. The foil of the specimens with lower relative densities does not have as much resistance to the creation of additional folds after the initial buckling is observed because the energy capacity is depleted as soon as multiple folds are created immediately after the initial fold has occurred.

A plot of compressive strength with respect to changing relative density for all three core heights of the stabilized and bare compression specimens is shown in Figure 1.6 (tabular data will be presented later while discussing the statistical analysis). The compressive strength is plotted with respect to relative density because the compressive properties are largely dependent on the contact area of the foil edges, and the relative density is a parameter that describes this contact area. It can be seen that compressive strength increases with increasing relative density, and the core height appears to have little effect on the compressive strength response of a given specimen type, a behavior that was also seen by Côté *et al* [1.3]. Although the effect is small, the results (for a given specimen type) do show that compressive strength increases with decreasing core height, as would be expected. The insensitivity to core height is possibly due to the fact that the honeycomb cell walls buckle in folds as was described earlier. Once the first fold is made the specimen begins to soften and successive folds of the same size are created until the test is terminated. The geometry of the first fold stays consistent as the cell wall height is increased, as long as the foil thickness and cell size are constant, so the force required to create the first fold (which is what dictates the maximum compressive strength) is insensitive to the core height. Images of failed specimens showing folds can be seen in Appendix B. The compressive strength plot also shows that the presence of

face sheets in the stabilized tests has a small, but noticeable effect on the compressive strength, where the stabilized specimens have a slightly lower compressive strength than the bare specimens. This is perhaps due to irregularities or misalignment in the bonded face sheet resulting in load concentrations on certain areas of the specimen cross-section.

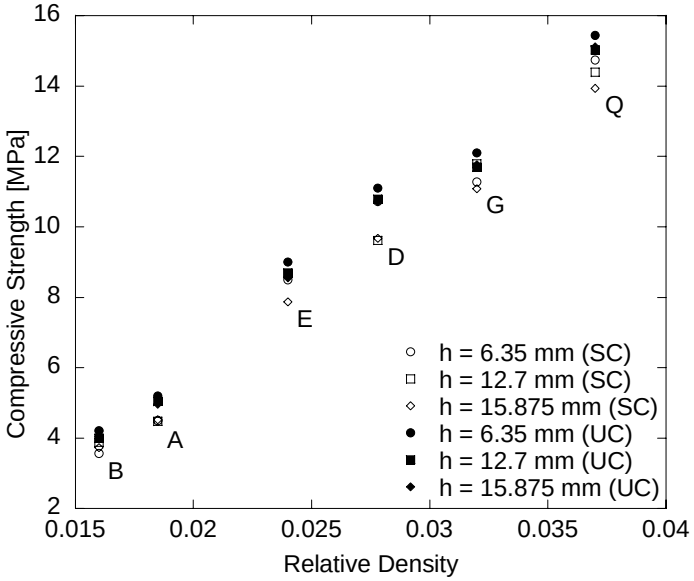

Figure 1.6: Compressive strength vs. relative density of the square cell titanium honeycomb (stabilized and bare compression tests)

Shown in Figure 1.7 are the compressive modulus results for all three core heights of stabilized and bare compression, with respect to changing relative density (tabular data will be presented later while discussing the statistical analysis). The compressive modulus appears to increase linearly with increasing relative density within each core height and specimen type. There is an inconsistency in the linear relationship for the bare specimens at a relative density of 0.0278 (configuration D). The compressive modulus at this relative density seems to be uncharacteristically larger than the linear trends for all other relative densities. It was noted that at configuration D, the tensile tests of the welds (quality control tests performed periodically by Benecor) were stronger than the other configurations, which could lead to the configuration D honeycomb being stiffer than expected. This inconsistency at configurations D can also be seen in the compressive strength data of Figure 1.6, but is not as apparent. The presence of a face sheet appears to have a more evident effect on compressive modulus; however, this may be due primarily

to the increase in the effect of core height. In contrast to the behavior of compressive strength, the compressive modulus is affected by varying core heights. As discussed for strength, the initial fold does not depend strongly on core height, so even if the core height increases, approximately the same amount of displacement is required to create the first fold. In other words, the slopes of the force-displacement curves are quite consistent among all specimens. However, when this displacement is converted to strain, the strain at failure is smaller for larger core heights, so the modulus increases. Both factors, the presence of face sheets and varying core heights, have an increasing effect on compressive modulus as the relative density increases. There is little published on the compressive modulus response of metallic honeycomb so there are no observations or explanations to draw on. Although not shown in Figures 1.6 and 1.7, it should be noted that the standard deviation for each group was larger for modulus than it was for strength. This will be discussed in more detail in the statistical analysis section.

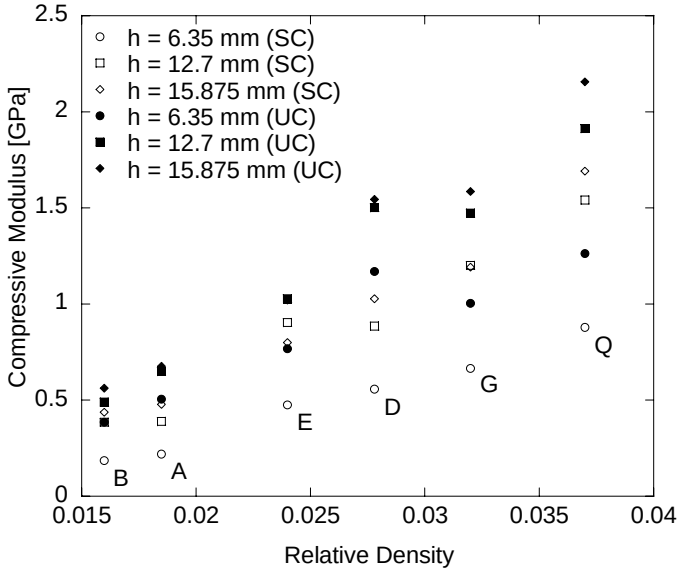

Figure 1.7: Compressive modulus vs. relative density of the square-cell titanium honeycomb (stabilized and bare compression tests)

Figure 1.8 shows the compressive strength with respect to changing relative density, plotted on a log-log scale. The data shown is the titanium square cell honeycomb from this study, as well as the stainless steel square cell honeycomb and aluminum hexagonal

honeycomb from the Côté *et al* study [1.3], which exhibits the increase in compressive strength with increase in relative density that was seen in the results of this study.

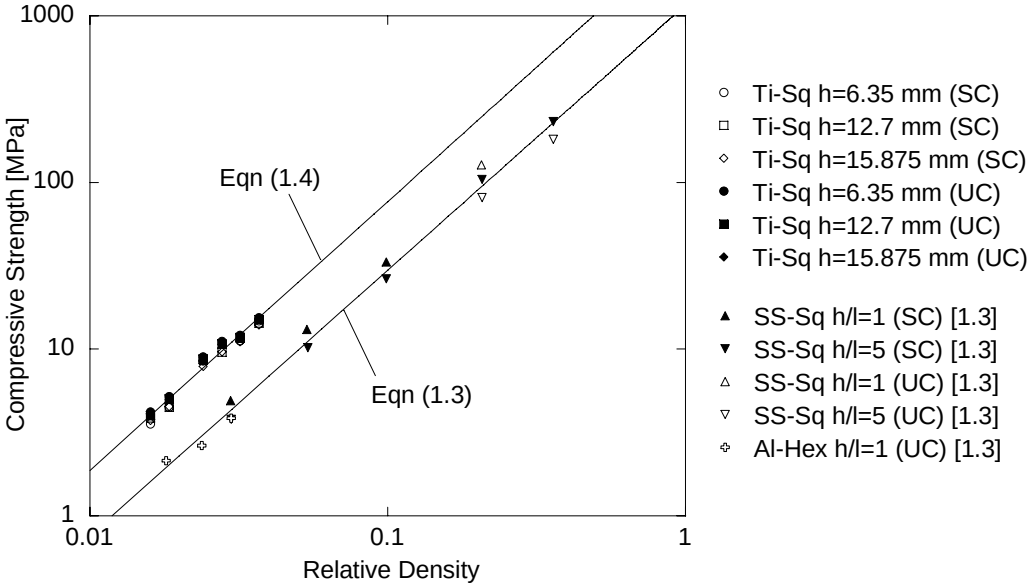

Figure 1.8: Compressive strength vs. relative density of the titanium honeycomb from this study, as well as stainless steel and aluminum honeycomb from Côté *et al* [1.3]

It can be seen in the figure that the titanium honeycomb has a linear behavior similar to that of the stainless steel and aluminum honeycomb, with the rate of increase about the same for the titanium as the stainless steel and aluminum honeycomb. The plot shows that the titanium honeycomb have a larger compressive strength than that of the aluminum or stainless steel honeycomb at each relative density, which is most likely due to the larger yield strength of titanium (910 MPa) compared to that of the stainless steel and aluminum used (210 MPa) [1.3]. However, the differences in manufacturing processes for the three types of honeycomb may also have a secondary affect. The compression strength difference appears to be constant throughout all relative densities when viewed on a log-log scale. A fit of the form

$$\sigma_c = 1161\bar{\rho}^{1.59} \tag{1.3}$$

best characterizes the compressive strength of both the stainless steel and aluminum honeycomb for all relative densities and all core heights evaluated in the Côté *et al*. study. Likewise, a fit of the form

$$\sigma_c = 3149\bar{\rho}^{1.61} \tag{1.4}$$

best characterizes the compressive strength of the titanium square cell honeycomb for all relative densities and all core heights evaluated in the current study. Both equations show that the slope of the two separate data sets is similar throughout the range of relative densities.

Statistical Analysis

A comprehensive statistical analysis at two different levels was performed on the data in this study. The first level was a basic numerical analysis and the second was a more detailed, statistical comparative analysis.

In the basic numerical analysis, mean and standard deviation values (for compressive strength and compressive modulus) were calculated for each group and are shown in Table 1.2. As previously discussed in Figures 1.6 and 1.7, and as seen in Table 1.2, the core height and specimen type both have slight effects on the compressive strength and modulus, with a larger influence from core height on compressive modulus. For example, to observe the small effect of core height on compressive strength in Table 1.2, the three core heights of a specimen type for a given configuration (e.g. A1SC, A2SC and A3SC) can be compared to each other to see the similarity of the three mean values, in the respective column for compressive strength. Although the level of scatter for each group cannot be seen in Figures 1.6 and 1.7, the mean and standard deviation in Table 1.2 can be used to determine the coefficient of variation (COV) of compressive strength and modulus for each group, where COV is the ratio of the standard deviation to the mean, expressed as a percent. Table 1.3 shows the distinctions between the stabilized and bare specimens as well as between the compressive strength and modulus that become apparent when comparing COVs. The increased variation within groups of stabilized specimens, as compared to groups of bare specimens, is best explained by a previous comment – the addition of a face sheet may introduce various defects to the structure.

Table 1.2: Numerical statistics summary for compressive strength and modulus for both bare and stabilized titanium square honeycomb (std dev = standard deviation, conf = confidence)

		Compressive Strength [MPa]				Compressive Modulus [GPa]			
		Basic		Mixed Model		Basic		Mixed Model	
Group	$\bar{\rho}$	Mean	Std Dev	Lower 95% Conf Limit	Upper 95% Conf Limit	Mean	Std Dev	Lower 95% Conf Limit	Upper 95% Conf Limit
B1SC	0.0160	3.6	0.4	3.0	4.1	0.19	0.08	0.09	0.28
B2SC		3.9	0.4	3.3	4.4	0.39	0.07	0.29	0.48
B3SC		3.7	0.3	3.2	4.3	0.44	0.10	0.34	0.53
A1SC	0.0185	4.5	0.7	4.0	5.1	0.22	0.10	0.13	0.31
A2SC		4.5	0.8	3.9	5.0	0.39	0.18	0.30	0.48
A3SC		4.5	0.4	4.0	5.1	0.48	0.14	0.38	0.57
E1SC	0.0240	8.5	0.9	7.9	9.1	0.48	0.18	0.38	0.57
E2SC		8.7	0.6	8.1	9.2	0.91	0.13	0.81	1.00
E3SC		7.9	0.7	7.3	8.4	0.80	0.16	0.71	0.89
D1SC	0.0278	10.7	1.6	10.2	11.3	0.56	0.24	0.46	0.65
D2SC		9.6	1.0	9.1	10.2	0.89	0.21	0.79	0.98
D3SC		9.7	1.3	9.1	10.2	1.03	0.31	0.94	1.12
G1SC	0.0320	11.3	1.5	10.7	11.8	0.66	0.23	0.57	0.76
G2SC		11.8	0.8	11.3	12.4	1.20	0.14	1.11	1.30
G3SC		11.1	1.1	10.5	11.6	1.19	0.21	1.10	1.29
Q1SC	0.0370	14.8	1.5	14.2	15.3	0.88	0.20	0.79	0.97
Q2SC		14.4	1.4	13.9	15.0	1.54	0.25	1.45	1.64
Q3SC		13.9	1.3	13.4	14.5	1.69	0.24	1.60	1.79
B1UC	0.0160	4.2	0.3	3.7	4.8	0.39	0.04	0.29	0.48
B2UC		4.0	0.3	3.5	4.6	0.49	0.07	0.40	0.58
B3UC		4.1	0.3	3.5	4.6	0.56	0.05	0.47	0.66
A1UC	0.0185	5.2	0.4	4.7	5.8	0.51	0.08	0.41	0.60
A2UC		5.0	0.4	4.5	5.6	0.65	0.07	0.56	0.74
A3UC		5.0	0.3	4.4	5.5	0.68	0.08	0.58	0.77
E1UC	0.0240	9.0	0.5	8.5	9.6	0.77	0.04	0.67	0.86
E2UC		8.7	0.4	8.1	9.2	1.03	0.10	0.93	1.12
E3UC		8.6	0.4	8.0	9.1	1.02	0.15	0.93	1.12
D1UC	0.0278	11.1	1.2	10.6	11.7	1.17	0.16	1.08	1.27
D2UC		10.8	1.1	10.2	11.3	1.50	0.21	1.41	1.60
D3UC		10.7	0.7	10.2	11.3	1.55	0.24	1.45	1.64
G1UC	0.0320	12.1	0.9	11.6	12.7	1.00	0.09	0.91	1.10
G2UC		11.7	0.7	11.1	12.3	1.47	0.14	1.38	1.57
G3UC		11.8	0.8	11.2	12.3	1.59	0.10	1.49	1.68
Q1UC	0.0370	15.4	1.2	14.9	16.0	1.26	0.11	1.17	1.36
Q2UC		15.0	1.1	14.5	15.6	1.91	0.15	1.82	2.01
Q3UC		15.1	1.1	14.6	15.7	2.16	0.10	2.06	2.25

Table 1.3: Numerical statistics comparison summary using COV of compressive strength and modulus values for each group of a given specimen type

	Minimum COV [%]	Maximum COV [%]	Mean COV [%]
SC Strength	6.39	16.88	10.76
SC Modulus	11.68	46.82	27.29
UC Strength	4.18	10.81	7.09
UC Modulus	4.78	15.74	10.62

In addition to calculating the means and standard deviations, a detailed statistical comparative analysis (linear mixed model in SAS®) was performed on the data. A linear mixed model is an extended form of an analysis of variance of several parameters, which can be defined as fixed effects (the specific values of the parameter have significance and importance) and/or random effects (the specific values of the parameter have no significance or importance). Fixed effects encompass both main effects and interactions, where main effects are individual parameters and interactions are relationships where changing one parameter has the potential to cause the influence of another parameter (or combination of parameters) on the given property to vary, symbolized by a "~" here. These interactions can be two-, three- or four-way (or more), depending on the test matrix of the study. From a linear mixed model analysis, confidence intervals can be obtained and the statistically significant main effects and interactions (i.e. the main effects and/or interactions that have a statistically significant influence on a given property) can be determined.

In general, in a linear mixed model all responses (data points) for a given property are fit to a mathematical model, whose design is dictated by the test matrix. The general form of a mathematical model has a single variable on the left-hand side to represent the property of interest, for a given combination of parameters. On the right-hand side of the model is an additive combination of terms, where the first term represents the overall mean of the property for the data set and each of the remaining terms represents a random error (or a set of discrete values corresponding to the influence of a fixed effect) on the

given property, for each value of the fixed effect. The discrete values of the influence terms will depend on how much influence the given fixed effect has on the property of interest and will add to or subtract from the overall mean in order to obtain a modified value which is representative of the mean value of a set of responses from samples with the same parameters. Each random error term has a normal distribution, a mean of zero and a variance different from any other random error terms, and therefore does not have discrete values.

The test matrix for this study was a completely randomized design with a split plot and subsampling on the split plot. The whole plot treatments were arranged in a 3x2 factorial design for the foil thickness and cell size, and the whole plot experimental unit was a block of material, with five blocks of material for each combination of foil thickness and cell size. The split plot treatments were arranged in a 3x2 factorial design for the core height and specimen type, where the split plot experimental units were the six batches that were taken from the same block. Finally, the subsamples were the specimens that came from each batch. More discussion of general linear model designs can be found in references such as [1.4, 1.5]. In this study, foil thickness, cell size, core height, and specimen type were treated as fixed effects and the batch numbers and associations with blocks of material were treated as random effects. The two properties of interest were compressive strength and modulus, each response was from a single specimen and the collection of responses with the same combination of parameters is the group of 30 specimens defined earlier.

The following mathematical model represents the linear model corresponding to the test matrix design in this study:

$$\begin{aligned} y_{ijuklt} = {} & \mu + FT_i + CS_j + (FT \sim CS)_{ij} + b_{iju} \\ & + CH_k + ST_l + (CH \sim ST)_{kl} \\ & + (CH \sim FT)_{ik} + (CH \sim CS)_{jk} + (CH \sim FT \sim CS)_{ijk} \\ & + (ST \sim FT)_{il} + (ST \sim CS)_{jl} + (ST \sim FT \sim CS)_{ijl} \\ & + (CH \sim ST \sim FT)_{ikl} + (CH \sim ST \sim CS)_{jkl} + (CH \sim ST \sim FT \sim CS)_{ijkl} \\ & + e_{ijukl} + s_{ijuklt} \end{aligned} \tag{1.5}$$

where i = 1, 2, 3 (number of foil thicknesses); j = 1, 2 (number of cell sizes); k = 1, 2, 3 (number of core heights); l = 1, 2 (number of specimen types); u = 1, …, 5 (number of blocks per configuration); t = 1, …, 6 (number of specimens per combinations of core height and specimen type within each block of each configuration). Here, y_{ijuklt} represents the material property (compressive strength or modulus) for a given specimen; μ is the overall mean of all of the responses for the given property; FT_i, CS_j, CH_k, ST_l are the influence terms for the main effects foil thickness, cell size, core height, and specimen type, respectively; b_{iju} is the block influence and serves as the whole plot error; e_{ijukl} serves as the split plot error; s_{ijuklt} is the subsample (specimen) influence and is also an error term; the other terms are influence terms for the interactions.

In this model, compressive strength and compressive modulus were analyzed separately. Shown in Table 1.2 for each group and for both properties are 95% confidence intervals based on the mixed model. These confidence intervals are larger than a basic statistical confidence interval calculation (based on standard deviations) would give, as the mixed model takes into account the variations in the entire set of data also and the test matrix design when determining confidence intervals for each group.

In the tests for statistically significant main effects, foil thickness, core height and specimen type were found to be statistically significant for compressive strength and compressive modulus, while the cell size was not identified as significant for either property. It should be noted that although core height seemed to have little effect on compressive strength, there was a slight visible trend in the compressive strengths with respect to core height, as discussed in Figure 1.6. Several two- and three-way interactions between fixed effects were detected as well.

For compressive strength, the statistically significant interactions were: (two-way) foil thickness and cell size; foil thickness and core height (marginally significant, i.e. $p < 0.10$); (three-way) foil thickness, cell size and specimen type. Table 1.4 summarizes these interactions. A key thing to note is that the interaction between foil thickness and cell size is related to relative density (based on Eqn (1.1)) and it is clear from Figure 1.6 that relative density has a significant effect on the compressive strength since the compressive strength increases as relative density increases. Similarly, the three-way

interaction between foil thickness, cell size and specimen type is related to the effect of specimen type with relative density. Again, this relationship can be seen in Figure 1.6 as the difference in compressive strength for stabilized and bare specimens increases as the relative density increases, keeping all other things constant (e.g. comparing a single core height in two different configurations where the only difference is cell size). The remaining interactions are not easily seen in Figure 1.6 or in Table 1.2. It should be noted that cell size was not identified as a significant main effect, even though it shows up in two of the three significant interactions for compressive strength. Therefore, it could be argued that cell size must be significant in order to be in a significant interaction. Excerpts from the SAS output for the analysis on compressive strength are shown in Appendix C.

Table 1.4: Statistically significant ($p < 0.05$) interactions between specimen parameters for compressive strength and modulus, where FT = foil thickness, CS = cell size, CH = core height, and ST = specimen type

	Compressive Strength	Compressive Modulus
2-way interactions	FT ~ CS FT ~ CH*	FT ~ CS FT ~ CH FT ~ ST CS ~ ST
3-way interactions	FT ~ CS ~ ST	FT ~ CS ~ CH FT ~ CS ~ ST

*Marginally significant interaction ($p < 0.10$)

Compressive modulus had the following statistically significant interactions: (two-way) foil thickness and cell size; foil thickness and core height; foil thickness and specimen type; cell size and specimen type; (three-way) foil thickness, cell size and core height; foil thickness, cell size and specimen type. These interactions are shown in Table 1.4. Similar to compressive strength, the compressive modulus also has the interaction between foil thickness and cell size (related to relative density), which can be seen in Figure 1.7 as the compressive modulus increases with increasing relative density.

Additionally, as previously discussed in Figure 1.7, the core height and the specimen type both have an increasing effect on the compressive modulus as the relative density increases. These relations are supported by the two significant three-way interactions for compressive modulus. Both interactions involved the foil thickness and cell size pair (representative of relative density) and the third parameter in each of the interactions is the core height or the stabilization, which corresponds to the two relations seen in Figure 1.7. The other interactions are not easily seen in Figure 1.7 or Table 1.2. As noted for compressive strength, cell size was not identified as a significant main effect, even though it shows up in several of the significant interactions for compressive modulus. Therefore, it could be argued here as well that cell size must be significant in order to be in a significant interaction. Excerpts from the SAS output for the analysis on compressive modulus are shown in Appendix C.

Further statistical comparative analyses to evaluate differences between batches and blocks were performed on the compressive strength and modulus properties obtained in this study. However, due to inconsistencies in the results, the evaluation of these differences is not reported.

Conclusion

The compression behavior of six different configurations of square cell titanium honeycomb was evaluated, according to ASTM standard C 365-05, and three different core heights of stabilized and bare specimens were tested for each configuration. The entire test matrix included 540 stabilized and 540 bare compression tests. It was found that the appearance of the stress-strain response is similar for stabilized and bare specimens at each relative density. The compressive strength as well as the compressive modulus increase with increasing relative density. The core height has little effect on the compressive strength, while the presence of a stabilizing face sheet has a small, but noticeable, effect on the compressive strength response. Additionally, the compressive modulus is affected by the core height and the presence of a face sheet, with increased effects on the specimens with larger relative densities. The compressive strength data was compared to stainless steel square cell and aluminum hexagonal cell honeycomb

from an existing study performed by Côté [1.3], and the two data sets appeared to have comparable trends. Both fit lines for compressive strength, seen in Figure 1.8, behaved with a similar slope; however, the titanium honeycomb, on the whole, had a larger compressive strength than both the stainless steel and aluminum honeycomb. At the completion of this study, a comprehensive statistical analysis of the data provided mean, standard deviation and 95% confidence intervals for each group tested, for both compressive strength and modulus. In addition, the main effects and interactions that were found to be statistically significant supported conclusions drawn from plots of the data and also provided some insight into the complex behaviors and interactions of the multiple parameters of the honeycomb.

References

1.1. Benecor, Inc. http://www.benecorinc.com/manufacturing.php. Wichita, KS.

1.2. ASTM International (2005) ASTM C 365 Standard Test Method for Flatwise Compressive Properties of Sandwich Cores. *Annual Book of Standards.* **15.03**. West Conshohocken, PA.

1.3. Cote, F., Deshpande, V.S., Fleck, N.A., and Evans, A.G. (2004) The Out-of-Plane Compressive Behavior of Metallic Honeycombs. *Materials Science and Engineering*. **A 380**, 272-280.

1.4 Littell, R.C., Milliken, G.A., Stroup, W.W., Wolfiryer, R.D. and Schabenberger, O. (2006) SAS for Mixed Models, 2nd Ed. SAS Institute, Inc., Cary, NC.

1.5 Mason, R.L., Gunst, R.F., and Hess, J.L. (1989) Statistical Design and Analysis of Experiments with Applications to Engineering and Science. Wiley-Interscience, New York, NY.

CHAPTER 3 – Shear Behavior of Square Cell Titanium Honeycomb*

Introduction

Most honeycomb cores are used in sandwich panel applications where they are bonded between two thin face sheets that carry an out-of-plane shear force, which is applied perpendicular to the walls that form the honeycomb cells. In this study, three different "orientations" of shear specimens were tested, where an orientation describes along what axis, relative to the cell walls, each specimen was sheared. The three orientations were defined as angle, ribbon and expansion which all corresponded to an axis in the plane of a specimen - the expansion axis is parallel to the direction that the honeycomb are expanded; the ribbon axis is parallel to the length of titanium foil, perpendicular to the expansion axis; the angle axis bisects the expansion and ribbon axes. All three axes are labeled in Figure 2.1, and the expansion process will be discussed in more detail in a following section.

This paper discusses the results of a rather large experimental program aimed at the characterization of shear properties of a laser welded square cell titanium honeycomb product, following ASTM C 273-06 *Standard Test Method for Shear Properties of Sandwich Core Materials* [2.1]. In this study a total of 1080 specimens were tested, with 360 specimens of each of the orientations. Multiple parameters were evaluated by varying the specimen cell size (l), core height (h), and foil thickness (t) (or cell wall thickness) which are shown in Figure 2.1. Each combination of cell size and foil thickness defines a "configuration", which includes three core heights and three orientations. This paper will also discuss the results of this program and a comprehensive statistical analysis of the data.

*This chapter is in the format of a manuscript intended for submittal to the *Journal of Experimental Mechanics*. Authors on this paper consist of Ryan Parsons, Elizabeth Frink, Kevin Lease, Suzanne Dubnicka, and Greg Jones.

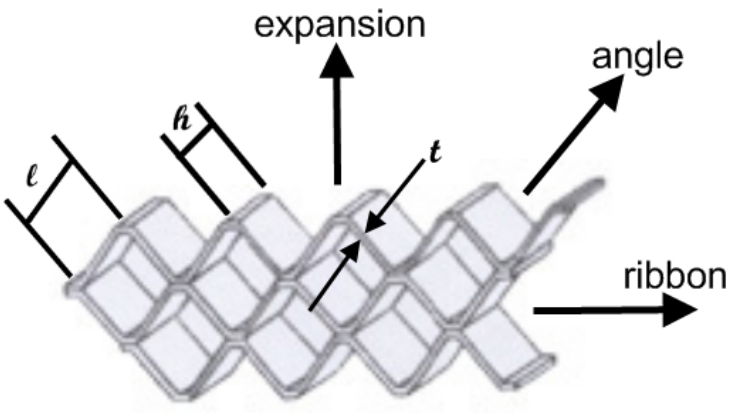

Figure 2.1: Illustration of square cell honeycomb labeling foil thickness (t), cell size (l), core height (h), and shearing orientations [2.2]

Material and Manufacturing Processes

The manufacturing process for the square cell titanium honeycomb in this paper involves a proprietary laser welding technique developed by Benecor Inc. (Wichita, KS). Benecor receives the ASTM certified Ti 3A1-2.5 2B annealed coil foil (nominal properties: σ_y = 910 MPa, E = 100 GPa, ν = 0.3) on oil free rolls of a specified foil thickness and width.

The manufacturing of the honeycomb core product involves several steps and begins with producing a "block" of foil material. Sheets are first cut from the titanium foil so that the length of foil removed from the roll is equal to the desired height (along the out-of-plane axis) of the block. The width of the roll of foil is the limiting factor for how wide a block can be. Two sheets are stacked, and then, using the proprietary laser welding process, a weld along the height of the sheets is made at predetermined intervals along the width of the sheets. The interval spacing determines the cell size of the honeycomb, and Benecor has developed a program that determines the laser welding interval for a given cell size. Each weld interval actually consists of several weld "spots", with a predetermined spacing, along the core height. Although the details of this spacing are proprietary, an example image is shown in Appendix A. At the end of each length of foil, the welding head returns to its start position for the next layer. Layer after layer of foil is welded until the required number of layers has been applied. At this point, the stacked and welded sheets are referred to as a block.

Each block is sliced into sections of the desired core height using a variety of metal cutting methods (e.g. EDM, water-jet), depending on the specified tolerance. The sliced section is then expanded (perpendicular to the surface of the sheets) to its full width and length (expansion direction) and is then referred to as a "blanket". Images of representative weld "nodes" can be seen in Appendix A. A weld node is the portion of foil length that is mated to another foil length creating a very strong point at the corner of each square cell. Final trim is performed (using an appropriate cutting method for the desired tolerance) to yield the final length and width requested by the customer.

In preparing the test specimens for this study, each blanket was hand-marked using templates made specifically to the ASTM standard specimen size requirements. Test specimens were then cut using a water cooled, diamond-encrusted (abrasive) blade. All specimens were 50.8 mm in width, with lengths of 76.2, 152.4, and 190.5 mm corresponding to 6.35, 12.7, and 15.875 mm core heights, respectively, to satisfy ASTM specimen size requirements. Pure shear tests of a honeycomb are not feasible because there is no way to grip a bare honeycomb specimen. For that reason, shear loading plates (platens) were adhered to the honeycomb faces to introduce a shear load to the core material, according to the test standard. For each core height there was a specific placement on the platens so that the load axis of the test machine passed through opposite edges of the specimen and the honeycomb orientation would correspond to one of the three shearing directions. The adhesive used to bond the core material to the platens was 3M's Scotch-Weld AF 163-2 cured at 250°F for one hour. All ASTM required dimensions were measured and recorded for each specimen, prior to adhering to shear platens.

In an attempt to evaluate differences between specimens from different blocks of material, a "group" of five "batches" of six specimens (cut from the same blanket) were tested for each foil thickness, cell size, core height and orientation combination that was tested. In each configuration the first batches came from the same block, and similarly for the remaining batches.

Test Matrix

The test matrix consisted of four different configurations and each configuration corresponds to a relative density, defined as:

$$\bar{\rho} = \frac{2t}{l}. \tag{2.1}$$

In this study, foil thicknesses of 0.025 and 0.038 mm, and cell sizes of 2.743 and 3.175 mm were used. Each configuration had three core heights: 6.35, 12.7, and 15.875 mm, and for each core height there were five batches of six specimens per orientation for a total of 270 specimens per configuration.

The four different configurations were designated by the letters B, A, E, and D (in order of increasing relative density). The configuration letter designations were chosen by the manufacturer to correspond to their existing labeling system. Table 2.1 shows the test matrix, which specifies the combination of foil thickness and cell size corresponding to each configuration. The core heights were assigned the numbers 01 thru 03 which corresponded to the three heights: 6.35, 12.7, and 15.875 mm respectively. To distinguish between the three orientations, the angle, ribbon, and expansion shear specimens were labeled "SA", "SR", and "SX" respectively. The batches were identified by the numbers 01 thru 05 and the individual specimens were identified by the numbers 01 thru 06. Each specimen was given an eight digit identification code, which consisted of the configuration letter, the core height number, the orientation designation, the batch number, and the individual specimen number. An example specimen identification code can be seen in Figure 2.2. The entire test matrix, summarized in Table 2.1, consisted of 360 angle shear tests, 360 ribbon shear tests and 360 expansions shear tests.

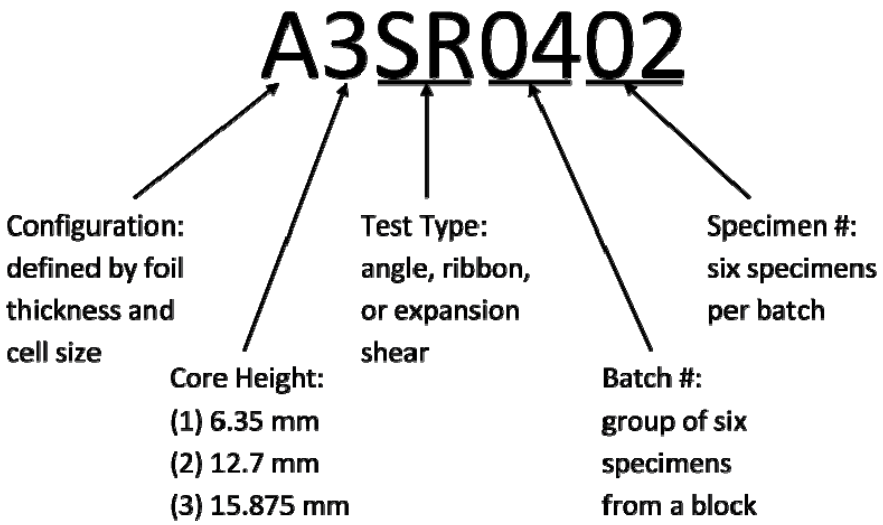

Figure 2.2: Example specimen identification code (this code is for the second ribbon shear specimen from configuration A, batch 04 with a 15.875 mm core height)

Table 2.1: Test matrix with relation to identification code conventions

Configuration	Foil Thickness [mm]	Cell Size [mm]	Relative Density	Core Height [mm] (designation)	# of Specimens (5 batches per thickness)		
					SA	SR	SX
B	0.025	3.175	0.016	6.35 (1)	30	30	30
				12.7 (2)	30	30	30
				15.875 (3)	30	30	30
A	0.025	2.743	0.019	6.35 (1)	30	30	30
				12.7 (2)	30	30	30
				15.875 (3)	30	30	30
E	0.038	3.175	0.024	6.35 (1)	30	30	30
				12.7 (2)	30	30	30
				15.875 (3)	30	30	30
D	0.038	2.743	0.028	6.35 (1)	30	30	30
				12.7 (2)	30	30	30
				15.875 (3)	30	30	30
				Total # of Tests	1080		

Experimental Procedure

The experimental procedure followed ASTM standard C 273-06, which covers the determination of shear properties of sandwich construction core materials associated with a shear load applied parallel to the loading platens. The core material can be bonded directly to the shear loading platens or to face sheets that are then bonded to the loading

platens. Also, the standard states that a tensile or compressive loading mode may be used. This paper will discuss honeycomb cores bonded directly to platens subjected to tensile loading.

All tests were performed at room conditions on a 245 kN Instron 8502 servo-hydraulic test machine using a shear fixture, seen in Figure 2.3, which consisted of two cantilevered pin-and-clevis-type fixtures attached to universal joints to ensure purely uni-axial loading of the pinned shear specimens. For stronger cores, additional plates were added to stabilize the free ends of the loading pins. Clamps were machined to hold an LVDT to measure the relative displacement between the two loading platens at the correct position on the specimens without hindering any movement during the test.

The tests were performed at a constant displacement rate, which varied for each configuration (0.305 mm/min for the smallest relative density to 1.067 mm/min for the largest relative density) to ensure that the samples failed in shear within the ASTM required time frame of three to six minutes. All analog signal data (force, crosshead displacement, and integrated LVDT) were recorded six times per second using a customized LabVIEW Virtual Instrument (VI). Along with the external signals, the VI was also programmed to automatically record the specimen number and the run-time as well as user inputs of specimen length, width, and thickness. The test date and test conditions (temperature and relative humidity) were also entered by the user and recorded. All signals and user inputs were saved to a spreadsheet file for documentation and data analysis.

Specimens were received from the industrial manufacturer with accompanying final measurements of the specimen length, width, and thickness recorded to three significant figures. Each specimen was loaded individually into the shear fixture and a pre-load of 90-135 N was applied to pull out any slack in the test fixture. The test rate was set at the appropriate value, and the displacement control test proceeded until the specimen had exhibited core shear failure. The ASTM standard specifies a three-place failure mode code, so that specimen failure can be properly and consistently reported. The ASTM failure mode code table can be seen in Appendix D. The only acceptable failure mode is core shear failure over the entire length of the honeycomb core material. Although some

specimens in this study exhibited unacceptable failure modes, these were all attributed to intermittent adhesive bond imperfections. Images of an acceptable failure and two unacceptable failures are shown in Appendix D.

Figure 2.3: Image of shear test fixture

Data Analysis

After the tests were completed, data analysis was performed on each raw data output file using a custom Microsoft Excel VBA macro. This analysis involved the calculation of

core instantaneous shear stress and strain, 2% offset shear strength, shear strength, and shear modulus as per ASTM C273-06 guidelines. The standard requires that the instantaneous core shear stress (τ) and strain (γ) throughout the test are calculated from the raw data as

$$\tau = \frac{P}{Lb} \tag{2.2}$$

$$\gamma = \frac{u}{h} \tag{2.3}$$

respectively, where P is the instantaneous force, L is the length of the specimen, b is the width of the specimen, u is the relative displacement, and h is the thickness of the core [2.1]. The ultimate shear strength (τ_{max}) is calculated using

$$\tau_{\max} = \frac{P_{\max}}{Lb} \tag{2.4}$$

where P_{max} is the maximum recorded force on the specimen [2.1]. The 2% offset shear strength (τ_{os}) is calculated for core materials that exhibit more than 2% shear strain by

$$\tau_{os} = \frac{P_{os}}{Lb} \tag{2.5}$$

where P_{os} is the 2% offset yield force [2.1]. Finally, the compressive modulus is defined as the slope of the linear region of the stress-strain curve and the suggested method for determining the core shear modulus involves a two-point slope calculation over the linear region of the force-displacement curve (illustrated between points A and B in Figure 2.4). However, in this study the slope is calculated using a linear regression due to the potential for increased accuracy and ease of implementation.

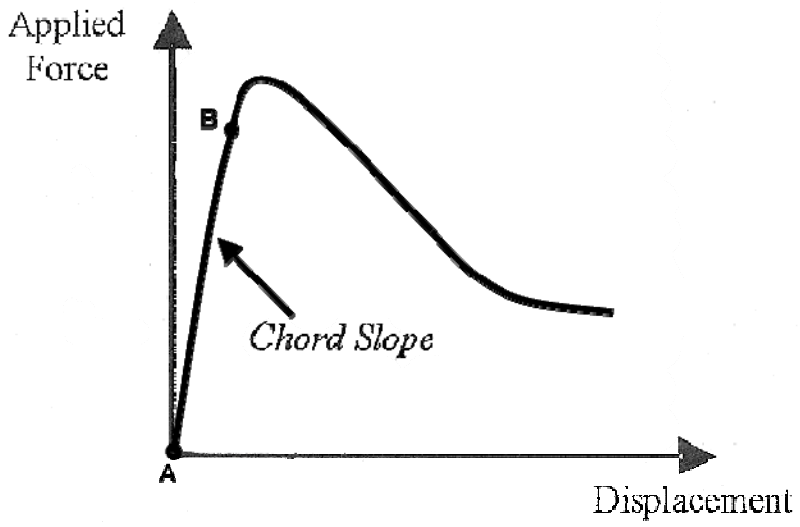

Figure 2.4: Illustration of force-displacement curve before manipulation showing the chord slope

From the raw data file, the macro separated the six tests of a given batch into six tabs in Excel and graphed the force-displacement and the stress-strain curve for each test. An interactive prompt allowed the user to view the force-displacement curves and define and appropriate linear region for the batch. A linear regression was performed on each test to determine the chord slope and the resulting shear modulus of each specimen. After calculation of all shear properties was completed for each test in a group, means and standard deviations of the shear strength and modulus were calculated, for each batch of 6 and the group of 30. A more thorough statistical analysis on the data set was performed when all configurations were completed and will be discussed in a later section of this paper.

Results and Discussion

Characteristic stress-strain curves for the three orientations of each configuration are shown in Figure 2.5. The appearance of the stress-strain curves varied slightly across the test matrix between configurations and orientations; however, all specimens displayed a somewhat similar trend for the general stress-strain response.

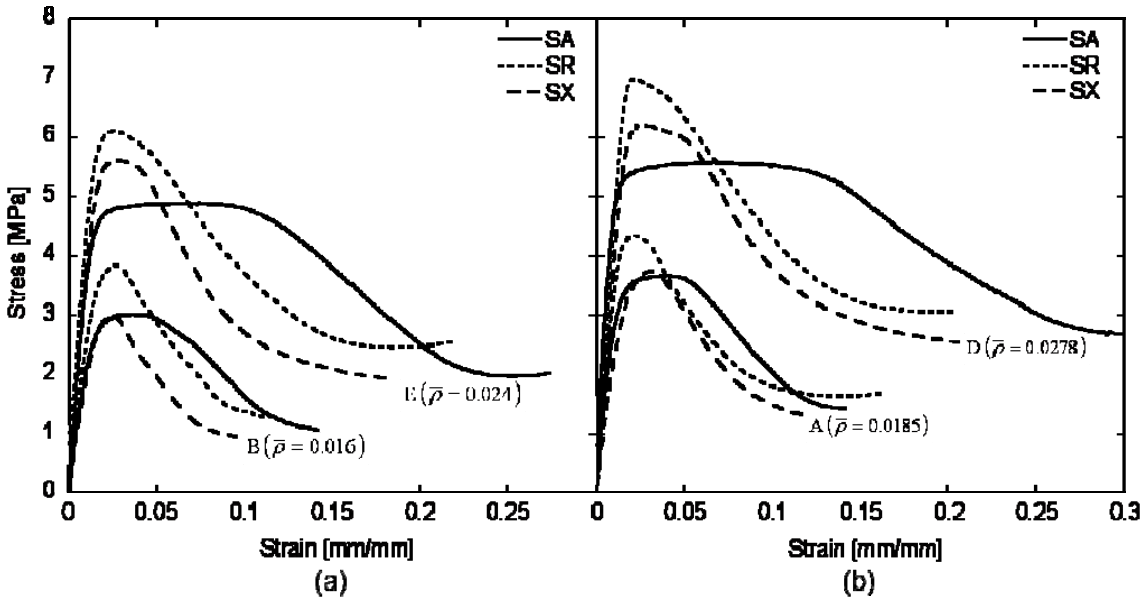

Figure 2.5: Characteristic stress-strain curves of configurations (a) A and D as well as (b) B and E (data from h=12.7 mm specimens)

The stress-strain curves started with a linear elastic region where the stress increased linearly with increasing strain to a maximum at which point the cell walls began to buckle. Following the maximum, the specimens began to deform and the curves entered a non-linear region as the stress decreased with increasing strain. This trend continued until the stress reached a plateau that remained constant until the tests were terminated. Shi-Dong [2.3] previously documented this stress-strain behavior as well. During plastic deformation of the specimens in this study, shear bands (bulges and creases) could be seen in the visible cell walls of the honeycomb specimens at 45° angles to the faces and platens similar to the behavior seen in previous studies [2.3, 2.4]. Images of failed specimens showing the shear bands can be seen in Appendix E

In looking more closely at differences between the general stress strain appearance described above, the honeycomb with larger relative density appeared to have a sharper transition from linear to non-linear behavior (as seen by configurations E and D in Figure 2.5). This is possibly due to the larger relative density honeycomb storing more energy while loading elastically so when the cell walls begin to buckle and release energy, the plastic deformation occurs more rapidly. Also, the SA orientation specimens in all configurations softened slower than the other orientations. The stress-strain curves of the

SA orientation tests show that the specimens were capable of sustaining a high post max stress as strain increased. This same behavior, to a lesser degree, was seen in the specimens with a large relative density (E and D). As relative density increased, the specimens seemed to soften slower.

The plots in Figure 2.5 show that the SR orientation is the strongest followed by the SX and then the SA orientations for all configurations. Referring to Figure 2.1, it can be seen that the SR orientation is shearing along the ribbon direction and the SX orientation is shearing along the expansion direction. At first glance it would appear that these two orientations would have the same shear response, but because of the influence of the weld node the responses are different. When a specimen is sheared in the ribbon direction, the weld node is sheared parallel to the lengths of foil that are mated. Conversely, for the expansion direction, the weld node is sheared perpendicular to the mated foil, which puts the weld node in a state of simple bending. The weld nodes are more resistant to a shearing force parallel to the mated foil than they are to a shearing force perpendicular to the mated foil, which is the reason for the SR shear specimens having a larger shear strength than the SX specimens. Likewise, the SA specimens are sheared in the angle direction where half of the cell walls are subjected to simple bending and the other half are subjected to pure shear. The cell walls are not very resistant to simple bending, which explains why the SA shear specimens have the smallest shear strength. This also explains why the SA specimens soften slower than the others. The SA specimen cell walls in pure shear do not release their energy as suddenly as the cell walls of the SR and SX specimens.

The strain at failure varied for each orientation and was also influenced by relative density and core height. The SR orientation failed at the lowest strain (most specimens ~2%) followed by the SX orientation (most specimens 2%~4%) then the SA orientation (most specimens 3%~6%). Within those ranges, the relative density also played a role in the strain at failure – as relative density increased, the failure strain increased for a given orientation. Additionally, within each configuration, the h=12.7 and 15.875 mm specimens had similar failure strains, holding everything else constant, but the h=6.35 mm specimens had a higher failure strain than the 12.7 and 15.875 mm specimens. The factor driving this difference in failure strain at only the shortest core height may be due

to the larger percentage of the core height influenced by the adhesive fillet at the honeycomb-adhesive interface of the h=6.35 mm specimens, which could alter the shear response and properties of the honeycomb material.

A plot of the shear strength with respect to changing relative density for all three core heights and all three orientations is shown in Figure 2.6 (tabular data will be presented later while discussing the statistical analysis). The plot shows that shear strength increases with increasing relative density and has a linear relationship with relative density within each core height and shear orientation. If all parameters are held constant, the shear strength decreases with increasing core height. This could be due to a larger bending moment in the cell walls for the larger core height specimens. Also, the h=6.35 mm specimen shear strengths increase the fastest with increasing relative density, followed by the 12.7 mm and 15.875 mm specimens respectively. This could be due to an increasing percentage of the core height filling with adhesive for the shortest specimens with the thickest foil and smallest cell size. As previously discussed in Figure 2.5, shear orientation has an effect on shear strength. There are few experimental results published on the shear strength of metallic honeycombs so this research area would greatly benefit from further extensive studies.

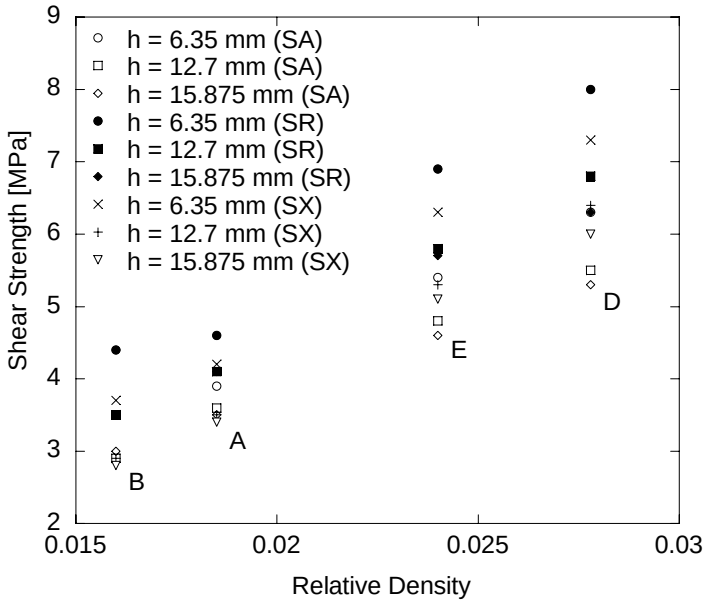

Figure 2.6: Shear strength vs. relative density of the square cell titanium honeycomb (SA, SR, and SX orientations)

Shown in Figure 2.7 is the shear modulus, for all three core heights and all three orientations, with respect to changing relative density (tabular data will be presented later while discussing the statistical analysis). Similar to the shear strength, the shear modulus increases with increasing relative density. The rate of increase of shear modulus with respect to relative density is proportional to core height. Although no clear trend is observed, orientation does seem to have an effect on shear modulus. Although not shown in Figures 1.6 and 1.7, it should be noted that the standard deviation for each group was larger for modulus than it was for strength. This will be discussed in more detail in the statistical analysis section.

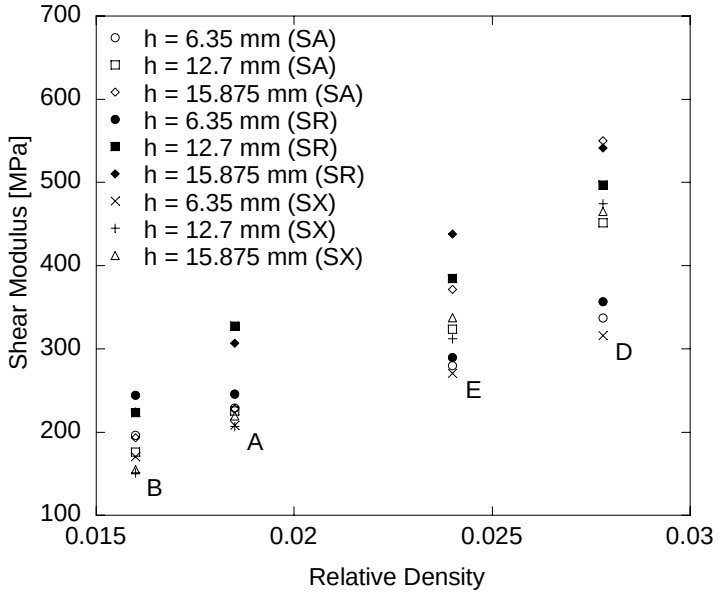

Figure 2.7: Shear modulus vs. relative density of the square cell titanium honeycomb (SA, SR, and SX orientations)

Figure 2.8 shows the shear modulus with respect to changing relative density plotted on a log-log scale. The data shown is the titanium square cell honeycomb as well as aluminum hexagonal cell honeycomb (ribbon orientation; h = 80 mm) from a study by Meraghni *et al* [2.5]. In order to compare the data sets, the relative density of the hexagonal honeycomb was calculated as

$$\overline{\rho}_{hex} = \frac{8}{3\sqrt{3}}\frac{t}{l} \tag{2.6}$$

with the given dimensions of the hexagonal cell honeycomb.

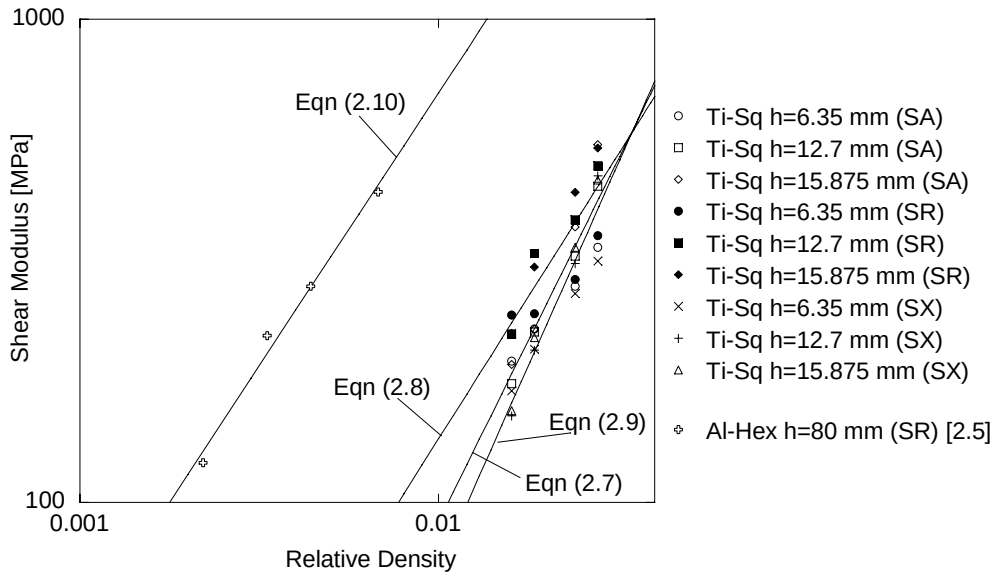

Figure 2.8: Shear modulus vs. relative density of the titanium honeycomb as well as aluminum honeycomb from Meraghni *et al* [2.5]

It can be seen that the shear modulus of the aluminum hexagonal honeycomb has a trend similar to that of the titanium square honeycomb. Fit lines of the form

$$\tau_{\max} = 89270\,\bar{\rho}^{1.50} \tag{2.7}$$

$$\tau_{\max} = 30353\,\bar{\rho}^{1.18} \tag{2.8}$$

$$\tau_{\max} = 160571\,\bar{\rho}^{1.67} \tag{2.9}$$

were found for the SA, SR, and SX orientations of this study, respectively. Also, a fit of the form

$$\tau_{\max} = 127676\,\bar{\rho}^{1.13} \tag{2.10}$$

was found for the aluminum hexagonal honeycomb from Meraghi et al [2.5]. It is interesting to note that the SR orientation fit line (Eqn (2.8)) has a slope that is similar to that of the aluminum honeycomb fit line (Eqn (2.10)), especially since the aluminum honeycomb in the Meraghni *et al* study was sheared in the same direction as the titanium SR specimens (ribbon). Even though the Meraghni *et al* honeycomb is aluminum hexagonal and has a much larger core height (80 mm) than all of the titanium square honeycomb in this study, the shear moduli follow a similar trend with respect to changing

relative density when comparing the ribbon orientations. The larger shear modulus of the aluminum specimens, in most part, is likely due to the manufacturing method and shearing direction of the aluminum honeycomb. The aluminum honeycomb are manufactured by forming the ribbons then welding them together, which causes all of the cell walls parallel to the ribbon direction to be double foil thickness and much stronger and stiffer. The specimens are then sheared parallel to the double walls creating a very large shear modulus.

Statistical Analysis

A comprehensive statistical analysis at two different levels was performed on the data in this study. The first level was a basic numerical analysis and the second was a more detailed, statistical comparative analysis.

In the basic numerical analysis, mean and standard deviation values (for shear strength and shear modulus) were calculated for each group and are shown in Table 2.2. As previously discussed in Figure 2.6, and as more clearly seen in Table 2.2, the shear strength decreases non-linearly as core height increases in each configuration. Also shown in this table is the trend that at a given core height SR has a larger shear strength than SX which has a larger shear strength than SA, for all configurations. Table 2.2 also illustrates the change in shear modulus due to change in core height, which was discussed in Figure 2.7; however, the increasing effect of the core height with increasing relative density is more difficult to see on the table. It should be noted that in the A2SR group, there was one specimen that exhibited a shear modulus approximately one-half of an order of magnitude larger than the mean shear moduli for all SR specimens tested in this study. This exceptionally large value was not removed from the data for data analysis and contributes to a significant portion of the standard deviation value for the A2SR group, and also artificially weights the mean value. If this exceptionally large value was removed before the numerical analysis, the mean shear modulus for A2SR would be 282 MPa and the standard deviation would be 51 MPa. The shear strength of this same specimen was within the region of the other five specimens in the A2SR group and did not have an effect on the shear strength numerical statistics of the group.

Table 2.2: Numerical statistics summary for shear strength and shear modulus for titanium square honeycomb in angle, ribbon and expansion orientations
(std dev = standard deviation, conf = confidence)

		Shear Strength [MPa]				Shear Modulus [MPa]			
		Basic		Mixed Model		Basic		Mixed Model	
Group	$\bar{\rho}$	Mean	Std Dev	Lower 95% Conf Limit	Upper 95% Conf Limit	Mean	Std Dev	Lower 95% Conf Limit	Upper 95% Conf Limit
B1SA	**0.0160**	3.5	0.1	3.3	3.8	196	33	170	222
B2SA		3.0	0.1	2.7	3.2	176	31	150	202
B3SA		3.0	0.1	2.8	3.2	193	22	168	219
A1SA	**0.0185**	3.9	0.2	3.7	4.2	229	33	203	255
A2SA		3.6	0.1	3.4	3.8	225	26	200	251
A3SA		3.5	0.2	3.3	3.7	228	24	202	254
E1SA	**0.0240**	5.4	0.2	5.2	5.7	280	31	254	306
E2SA		4.8	0.2	4.6	5.0	324	28	298	349
E3SA		4.6	0.1	4.4	4.8	372	54	346	398
D1SA	**0.0278**	6.3	0.3	6.1	6.5	338	33	312	363
D2SA		5.5	0.1	5.3	5.7	452	58	426	478
D3SA		5.3	0.1	5.1	5.5	551	90	525	577
B1SR	**0.0160**	4.4	0.7	4.2	4.6	245	44	219	270
B2SR		3.5	0.1	3.3	3.8	224	42	198	249
B3SR		3.5	0.2	3.3	3.7	224	19	199	250
A1SR	**0.0185**	4.6	0.2	4.4	4.8	246	24	220	272
A2SR		4.1	0.3	3.9	4.4	328	254	302	354
A3SR		4.1	0.2	3.9	4.4	307	46	281	333
E1SR	**0.0240**	6.9	0.4	6.7	7.1	290	24	264	316
E2SR		5.8	0.2	5.5	6.0	385	64	359	411
E3SR		5.7	0.3	5.4	5.9	438	95	413	464
D1SR	**0.0278**	8.0	0.5	7.8	8.2	357	44	331	383
D2SR		6.8	0.3	6.6	7.0	497	64	472	523
D3SR		6.3	0.8	6.1	6.5	542	61	516	568
B1SX	**0.0160**	3.7	0.2	3.5	4.0	171	26	145	196
B2SX		2.9	0.1	2.7	3.1	151	12	125	177
B3SX		2.8	0.1	2.6	3.1	155	20	129	181
A1SX	**0.0185**	4.2	0.2	4.0	4.5	208	33	182	234
A2SX		3.5	0.2	3.3	3.7	207	34	181	233
A3SX		3.4	0.2	3.2	3.7	220	57	194	245
E1SX	**0.0240**	6.3	0.3	6.1	6.6	271	29	245	297
E2SX		5.3	0.1	5.1	5.5	313	37	287	338
E3SX		5.1	0.2	4.9	5.3	338	23	312	364
D1SX	**0.0278**	7.3	0.3	7.1	7.6	316	30	290	342
D2SX		6.4	0.5	6.2	6.6	475	90	449	501
D3SX		6.0	0.3	5.8	6.2	465	34	439	491

Table 2.3: Numerical statistics comparison summary using COV of shear strength and modulus values

	Minimum COV [%]	Maximum COV [%]	Mean COV [%]
Shear Strength	2.39	15.25	4.91
Shear Modulus	6.95	26.10	13.49

Although the level of scatter for each group cannot be seen in Figures 2.6 and 2.7, the mean and standard deviation in Table 2.2 can be used to determine the coefficient of variation (COV) of shear strength and modulus for each group, where COV is the ratio of the standard deviation to the mean, expressed as a percent. Table 2.3 shows the distinction between the shear strength and modulus that becomes apparent when comparing COVs (with the previously mentioned value in A2SR removed from the data).

In addition to calculating the means and standard deviations, a detailed statistical comparative analysis (linear mixed model in SAS®) was performed on the data A linear mixed model is an extended form of an analysis of variance of several parameters, which can be defined as fixed effects (the specific values of the parameter have significance and importance) and/or random effects (the specific values of the parameter have no significance or importance). Fixed effects encompass both main effects and interactions, where main effects are individual parameters and interactions are relationships where changing one parameter has the potential to cause the influence of another parameter (or combination of parameters) on the given property to vary, symbolized by a "~" in later equations. These interactions can be two-, three- or four-way (or more), depending on the test matrix of the study. From a linear mixed model analysis, confidence intervals can be obtained and the statistically significant main effects and interactions (i.e. the main effects and/or interactions that have a statistically significant influence on a given property) can be determined.

In general, in a linear mixed model all responses (data points) for a given property are fit to a mathematical model, whose design is dictated by the test matrix. The general form of a mathematical model has a single variable on the left-hand side to represent the property of interest, for a given combination of parameters. On the right-hand side of the

model is an additive combination of terms, where the first term represents the overall mean of the property for the data set and each of the remaining terms represents a random error (or a set of discrete values corresponding to the influence of a fixed effect) on the given property, for each value of the fixed effect. The discrete values of the influence terms depend on how much influence the given fixed effect has on the property of interest and will add to or subtract from the overall mean in order to obtain a modified value which is representative of the mean value of a set of responses from samples with the same parameters. Each random error term has a normal distribution, a mean of zero and a variance different from any other random error terms, and therefore does not have discrete values.

The test matrix for this study was a completely randomized design with a split plot and subsampling on the split plot. The whole plot treatments were arranged in a 3x2 factorial design for the foil thickness and cell size, and the whole plot experimental unit was a block of material, with five blocks of material for each combination of foil thickness and cell size. The split plot treatments were arranged in a 3x2 factorial design for the core height and orientation, where the split plot experimental units were the six batches that were taken from the same block. Finally, the subsamples were the specimens that came from each batch. More discusion of general linear model designs can be found in references such as [2.6, 2.7]. In this study, foil thickness, cell size, core height, and orientation were treated as fixed effects and the batch numbers and associations with blocks of material were treated as random effects. The two properties of interest were shear strength and modulus, each response was from a single specimen and the collection of responses with the same combination of parameters is the group of 30 specimens defined earlier.

The following mathematical model represents the linear model corresponding to the test matrix design in this study:

$$
\begin{aligned}
y_{ijuklt} = {} & \mu + FT_i + CS_j + (FT \sim CS)_{ij} + b_{iju} \\
& + CH_k + O_l + (CH \sim O)_{kl} \\
& + (CH \sim FT)_{ik} + (CH \sim CS)_{jk} + (CH \sim FT \sim CS)_{ijk} \\
& + (O \sim FT)_{il} + (O \sim CS)_{jl} + (O \sim FT \sim CS)_{ijl} \\
& + (CH \sim O \sim FT)_{ikl} + (CH \sim O \sim CS)_{jkl} + (CH \sim O \sim FT \sim CS)_{ijkl} \\
& + e_{ijukl} + s_{ijuklt}
\end{aligned} \tag{2.11}
$$

where i = 1, 2, 3 (number of foil thicknesses); j = 1, 2 (number of cell sizes); k = 1, 2, 3 (number of core heights); l = 1, 2, 3 (number of orientations); u = 1, …, 5 (number of blocks per configuration); t = 1, …, 6 (number of specimens per combinations of core height and orientation within each block of each configuration). Here, y_{ijuklt} represents the material property (shear strength or modulus) for a given specimen; μ is the overall mean of all of the responses for the given property; FT_i, CS_j, CH_k, O_l are the influence terms for the main effects foil thickness, cell size, core height, and orientation, respectively; b_{iju} is the block influence and serves as the whole plot error; e_{ijukl} serves as the split plot error; s_{ijuklt} is the subsample (specimen) influence and is also an error term; the other terms are influence terms for the interactions.

In this model, shear strength and shear modulus were analyzed separately. Shown in Table 2.2 for each group and for both properties are 95% confidence intervals based on the mixed model. These confidence intervals are larger than a basic statistical confidence interval calculation (based on standard deviations) would give, as the mixed model takes into account the variations in the entire set of data and also the test matrix design when determining confidence intervals for each group. As previously noted, there was a specimen with an exceptionally large modulus value in A2SR, which also artificially weights the confidence intervals.

In the tests for statistically significant main effects (i.e. a fixed effect that has a statistically significant effect on a given property), foil thickness, cell size, core height and orientation were all found to be statistically significant for shear strength and shear modulus. Several significant two-, three-, and four-way interactions between fixed effects were detected as well.

For shear strength the statistically significant interactions were: (two-way) foil thickness and cell size; foil thickness and core height; foil thickness and orientation; core height and orientation; (three-way) foil thickness, cell size and core height. Table 2.4 summarizes these interactions. A key thing to note is that the interaction between foil thickness and cell size is related to relative density (based on equation (2.1)) and it is clear from Figure 2.6 that relative density has a significant effect on the shear strength. Similarly, the three-way interaction between foil thickness, cell size and core height is related to the effect of core height with relative density. Again, this relationship can be seen in Figure 2.6 and Table 2.2 as the difference between shear strengths of a given configuration (or relative density) increases (non-linearly) as the core height increases. The remaining significant interactions are not clearly visible in Figure 2.6 or Table 2.2. Excerpts from the SAS output for the analysis on shear strength are shown in Appendix F.

Table 2.4: Statistically significant ($p < 0.05$) interactions between specimen parameters for shear strength and shear modulus, where FT = foil thickness, CS = cell size, CH = core height, and O = orientation

	Shear Strength	Shear Modulus
2-way interactions	FT ~ CS FT ~ CH FT ~ O CH ~ O	FT ~ CS FT ~ CH CS ~ CH CH ~ O FT ~ O*
3-way interactions	FT ~ CS ~ CH	FT ~ CH ~ O FT ~ CS ~ O*
4-way interactions	--	FT ~ CS ~ CH ~ O

*Marginally significant interaction ($p < 0.10$)

Shear modulus had the following statistically significant interactions: (two-way) foil thickness and cell size; foil thickness and core height; cell size and core height; core height and orientation; foil thickness and orientation (marginally significant, i.e. $p < 0.10$); (three-way) foil thickness, core height and orientation; foil thickness, cell size and orientation (marginally significant); (four-way) foil thickness, cell size, core height and orientation. These interactions are shown in Table 2.4. Similar to shear strength, the shear modulus also has the interaction between foil thickness and cell size (related to relative density), which can be seen in Figure 2.7 as the shear modulus increases with increasing relative density. Although somewhat complicated, the four-way interaction was also (partially) described in Figure 2.7. In this interaction, the foil thickness and cell size are related to relative density and the increasing effect of core height can be seen in Figure 2.7. However, the fourth effect in this interaction is orientation and it is difficult to distinguish this additional influence in the figure. The other significant interactions for shear modulus are not easily observed in Figure 2.7 or Table 2.2. Excerpts from the SAS output for the analysis on shear modulus are shown in Appendix F.

Further statistical comparative analyses were performed on the shear strength and modulus properties obtained in this study. However, due to inconsistencies in the results, these evaluations of differences between batches and blocks are not reported.

Conclusion

Four different relative densities of square cell titanium honeycomb were shear tested according to AS

TM C 273-06. Three different core heights and three different shear orientations were tested for each relative density. The entire test matrix included 360 SA, 360 SR, and 360 SX shear tests. It was found that the shear strength as well as the shear modulus increased with increasing relative density. The shear strength of honeycomb decreased with increasing core height. Also, the SR (ribbon) orientation specimens had the largest shear strength throughout all relative densities. The core height appeared to have a small effect on the shear modulus - the rate of increase in shear modulus with respect to relative

density increased with increasing core height. The shear modulus data was compared to aluminum hexagonal cell honeycomb from an existing study performed by Meraghni *et al* The SR shear modulus data appeared to have the strongest correlation to the Meraghni *et al* data [2.5]. The fit lines of both sets of data behaved with a similar slope; however, the aluminum honeycomb, on the whole, had a larger shear modulus than the titanium honeycomb. At the completion of this study, a comprehensive statistical analysis of the data provided mean, standard deviation and 95% confidence intervals for each group tested, for both shear strength and modulus. In addition, the main effects and interactions that were found to be statistically significant supported conclusions drawn from plots of the data and also provided some insight into the complex behaviors and interactions of the multiple parameters of the honeycomb.

References

2.1. ASTM International (2006) ASTM C 273 Standard Test Method for Shear Properties of Sandwich Core Materials. *Annual Book of Standards.* **15.03**. West Conshohocken, PA.

2.2. Benecor, Inc. http://www.benecorinc.com/manufacturing.php. Wichita, KS

2.3. Shi-Dong, Pan. (2006) Longitudinal Shear Strength and Failure Process of Honeycomb Cores. *Composite Structures*. **72**, 42-46.

2.4. Zhang, J., Ashby M.F. (1992) Out-of-Plane Properties of Honeycombs. *International Journal of Mechanical Sciences*. **34**, 475-489.

2.5. Meraghni, F., Desrumaux, F., Benzeggagh, M.L. (1999) Mechanical Behavior of Cellular Core for Structural Sandwich Panels. *Composites: Part A*. **30**, 767-779.

2.6 Littell, R.C., Milliken, G.A., Stroup, W.W., Wolfiryer, R.D. and Schabenberger, O. (2006) SAS for Mixed Models, 2nd Ed. SAS Institute, Inc., Cary, NC.

2.7 Mason, R.L., Gunst, R.F., and Hess, J.L. (1989) Statistical Design and Analysis of Experiments with Applications to Engineering and Science. Wiley-Interscience, New York, NY.

CHAPTER 4 – Conclusion

This thesis discussed the results of a rather large experimental program aimed at the characterization of compressive and shear properties of a total of 2160 square cell titanium honeycomb specimens. The compressive study included the evaluation of six different configurations of titanium honeycomb according to ASTM standard C 365-05 while the shear study included four configurations that were evaluated according to ASTM standard C 273-06. Multiple parameters were tested by varying the foil thickness, cell size, and core height. After completion of all relevant data analysis, a comprehensive statistical analysis was performed on the strength and modulus properties of both shear and compression.

It was found that the appearance of the stress-strain response is similar for stabilized and bare compression specimens at each relative density. Conversely, the stress-strain response of the shear specimens varied between shear orientations. It was shown that both compressive and shear strengths and moduli increased with increasing relative density. The specimen core height had little effect on the compressive strength while the shear strength decreased with increasing core height. The compressive and shear moduli were both slightly affected by the core height - the rate of increase of the shear modulus with respect to relative density increased with increasing core height. The presence of face sheets on the compression specimens had a small but noticeable effect on the compressive strength and had an increasing effect on modulus with increasing relative density. Shear strength and modulus were both affected by the shearing orientation. The shear strength was most affected by the orientation, with the SR orientation having the largest shear strength followed by the SX and SA orientations respectively. Both sets of data, compressive and shear, were compared and found to have some similarities to existing experimental data. The compressive strength was compared to a study performed by Côté [1.3] while the shear modulus was compared to a study performed by Meraghni [2.5].

Two more configurations are scheduled to be shear tested to complete the first phase of the JSF contract, and more compression and shear testing will be completed outside of these configurations. Beam flexure and tensile tests (at room temperature and humidity, as well as elevated temperature and humidity tests and low temperature tests) for the second phase will also begin soon, and the results will be documented in a similar manner.

Appendix A

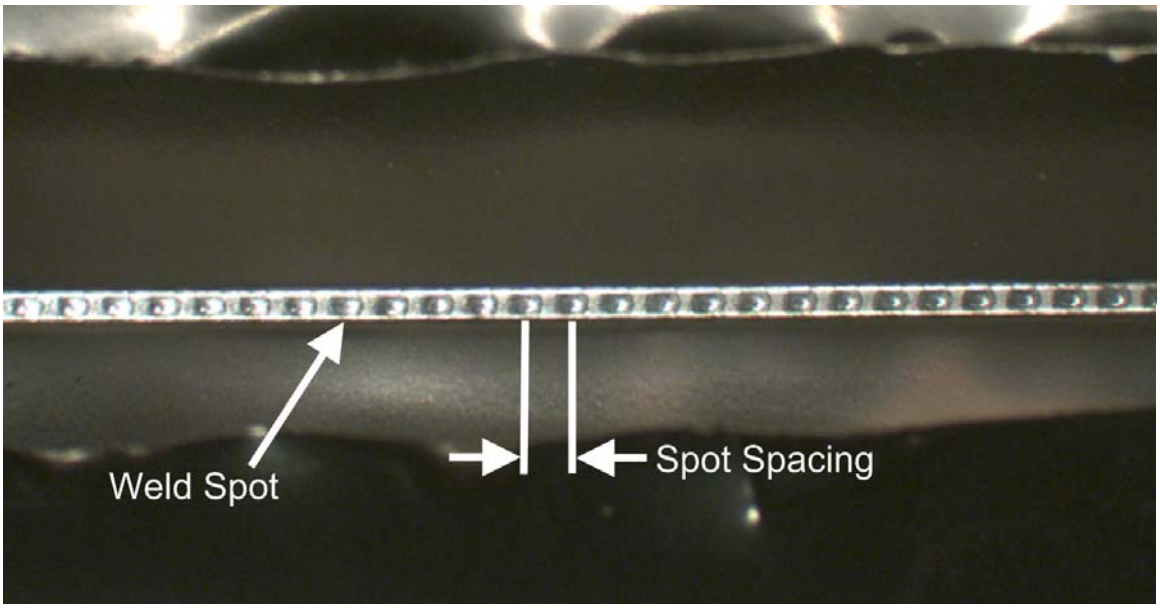

Figure A.1: Image of laser weld spot and weld spacing

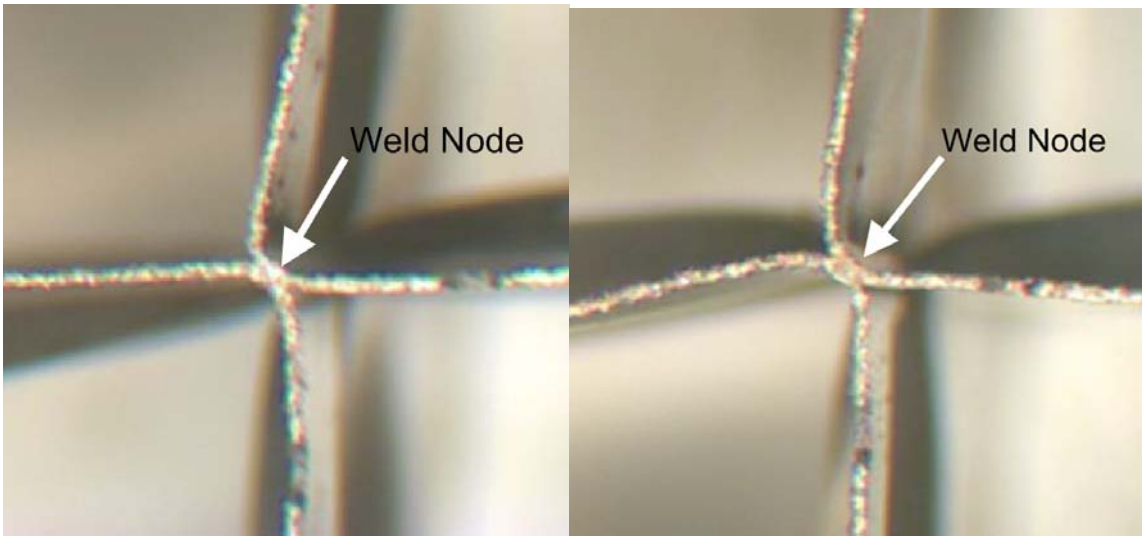

Figure A.2: Images of laser weld

Appendix B

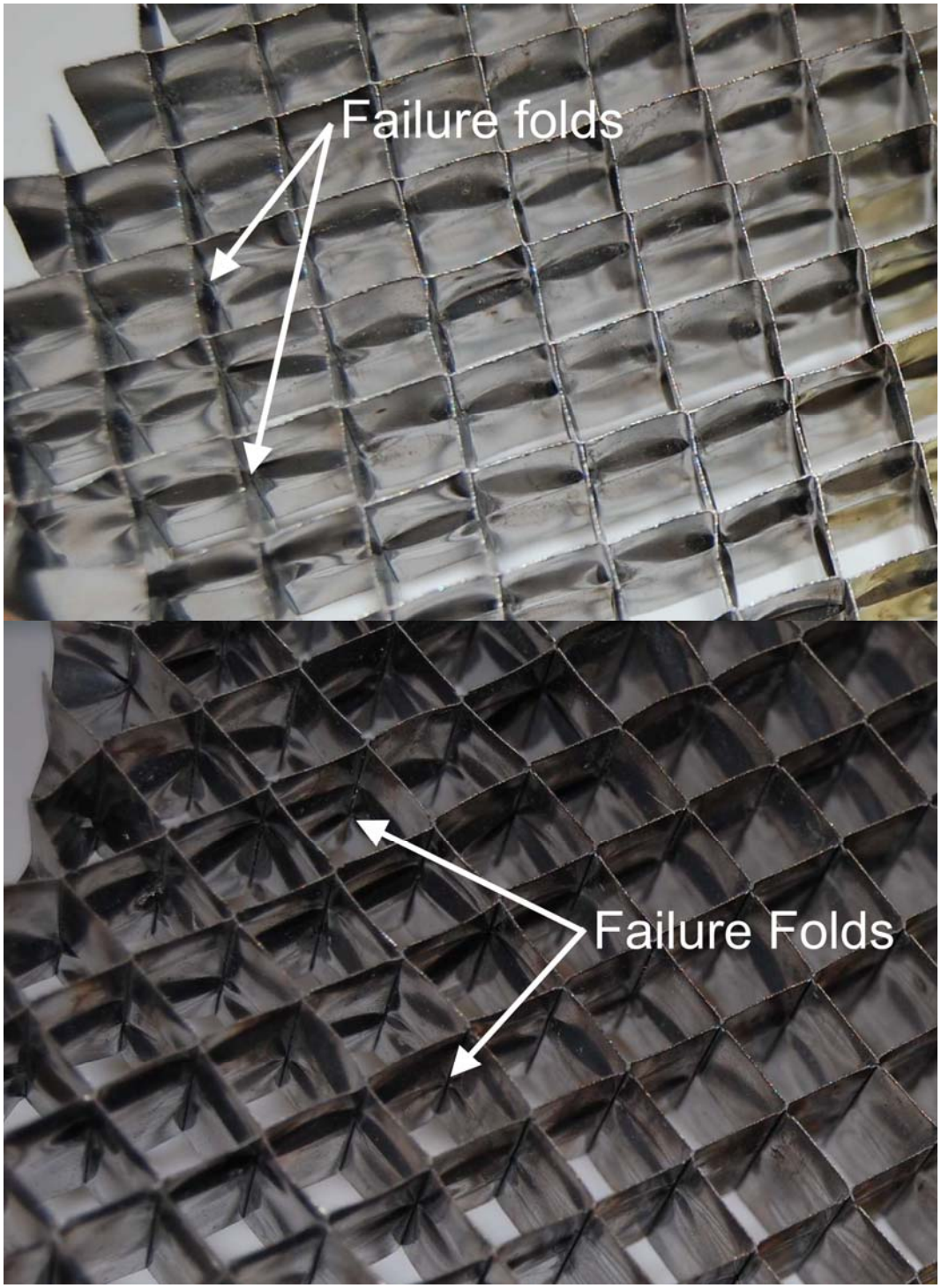

Figure B.1: Images of failure folds in bare compression specimens

Appendix C

Excerpts from SAS Output Results for Compressive Properties

Model Information

Data Set	WORK.COMPRESSION
Dependent Variable	**US (compressive strength)**
Covariance Structure	Variance Components
Estimation Method	REML
Residual Variance Method	Profile
Fixed Effects SE Method	Model-Based
Degrees of Freedom Method	Satterthwaite

Class Level Information

Class	Levels	Values
FT	3	0.001 0.0015 0.002
CS	2	0.108 0.125
CH	3	1 2 3
O	2	SC UC
B	5	1 2 3 4 5
S	6	1 2 3 4 5 6

Dimensions

Covariance Parameters	3
Columns in X	144
Columns in Z	210
Subjects	1
Max Obs Per Subject	1080

Number of Observations

Number of Observations Read	1080
Number of Observations Used	1080
Number of Observations Not Used	0

Type 3 Tests of Fixed Effects

Effect	**Num DF**	**Den DF**	**F Value**	**Pr > F**

FT	**2**	**24**	**965.78**	**<.0001 ***
CS	**1**	**24**	**0.61**	**0.4414**
FT*CS	**2**	**24**	**87.10**	**<.0001 ***
CH	**2**	**120**	**9.24**	**0.0002 ***
FT*CH	**4**	**120**	**2.12**	**0.0829 ****
CS*CH	**2**	**120**	**0.34**	**0.7128**
FT*CS*CH	**4**	**120**	**1.77**	**0.1399**
O	**1**	**120**	**70.92**	**<.0001 ***
FT*O	**2**	**120**	**0.70**	**0.4970**
CS*O	**1**	**120**	**0.55**	**0.4583**
FT*CS*O	**2**	**120**	**3.18**	**0.0450 ***
CH*O	**2**	**120**	**1.93**	**0.1492**
FT*CH*O	**4**	**120**	**1.29**	**0.2767**
CS*CH*O	**2**	**120**	**0.48**	**0.6177**
FT*CS*CH*O	**4**	**120**	**1.71**	**0.1524**

Model Information

Data Set	WORK.COMPRESSION
Dependent Variable	**Mod (compressive modulus)**
Covariance Structure	Variance Components
Estimation Method	REML
Residual Variance Method	Profile
Fixed Effects SE Method	Model-Based
Degrees of Freedom Method	Satterthwaite

Class Level Information

Class	Levels	Values
FT	3	0.001 0.0015 0.002
CS	2	0.108 0.125
CH	3	1 2 3
O	2	SC UC
B	5	1 2 3 4 5
S	6	1 2 3 4 5 6

Dimensions

Covariance Parameters	3
Columns in X	144
Columns in Z	210
Subjects	1
Max Obs Per Subject	1080

Number of Observations

Number of Observations Read	1080
Number of Observations Used	1080
Number of Observations Not Used	0

Type 3 Tests of Fixed Effects

Effect	Num DF	Den DF	F Value	Pr > F	
FT	2	24	427.38	<.0001	*
CS	1	24	0.11	0.7387	
FT*CS	2	24	57.45	<.0001	*
CH	2	120	434.81	<.0001	*
FT*CH	4	120	51.94	<.0001	*
CS*CH	2	120	2.10	0.1265	
FT*CS*CH	4	120	9.03	<.0001	*
O	1	120	645.05	<.0001	*
FT*O	2	120	25.15	<.0001	*
CS*O	1	120	28.55	<.0001	*
FT*CS*O	2	120	25.75	<.0001	*
CH*O	2	120	1.98	0.1426	
FT*CH*O	4	120	1.48	0.2120	
CS*CH*O	2	120	0.99	0.3760	
FT*CS*CH*O	4	120	0.78	0.5411	

Appendix D

Table D.1: ASTM specified three-place failure mode code [2.1]

First Character		Second Character		Third Character	
Failure Type	Code	Failure Area	Code	Failure Location	Code
Core Shear	S	At End	A	Top	T
Interface failure	I	Gage (within core)	G	Middle	M
Explosive	X	One Corner	C	Bottom	B
Other	O	Various	V	Entire Length	E
		Unknown	U	Various	V
				Unknown	U

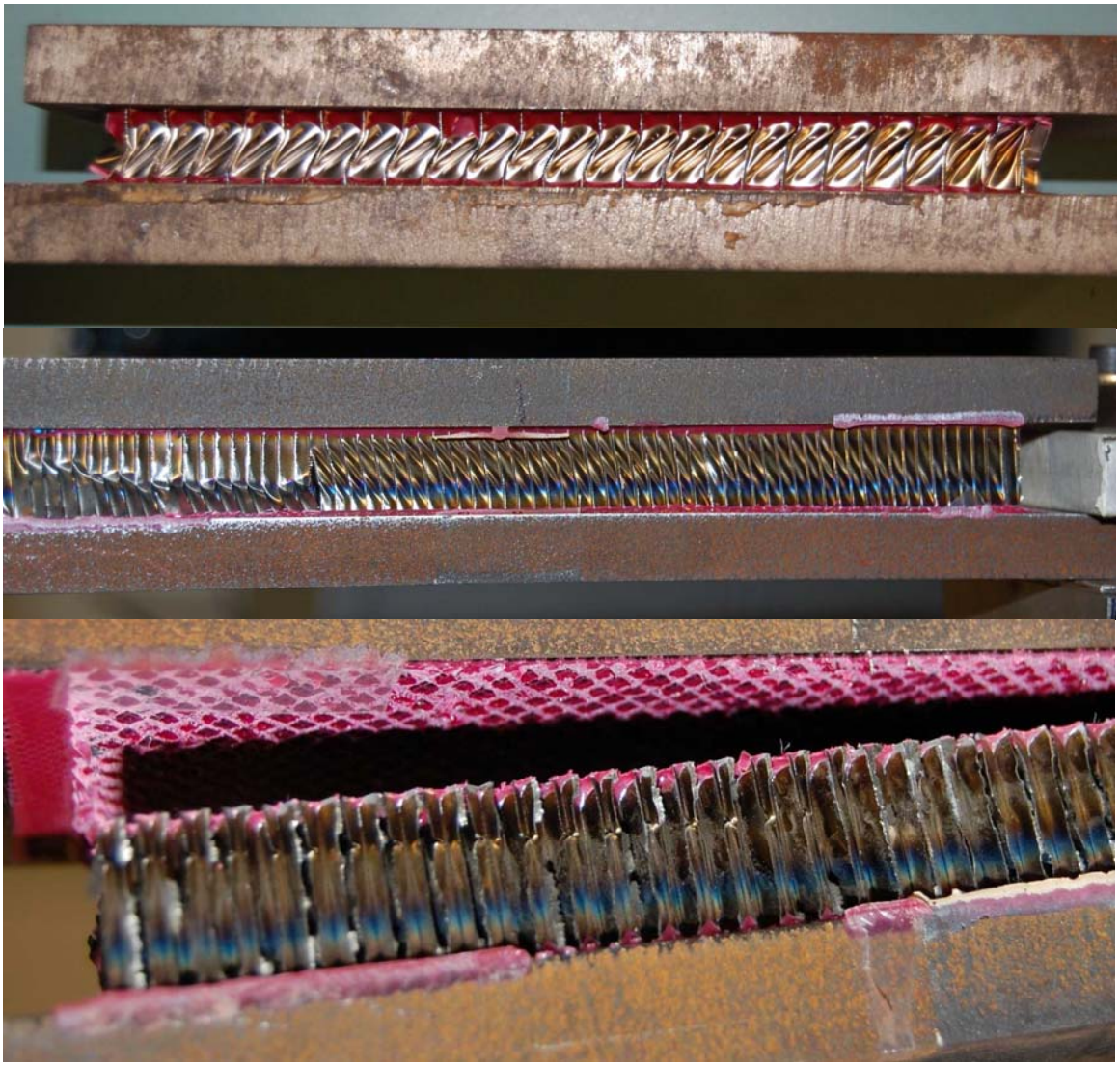

Figure D.1: Images of specimens with failure codes (a) SGE, (b) SGV, and (c) IVE

Appendix E

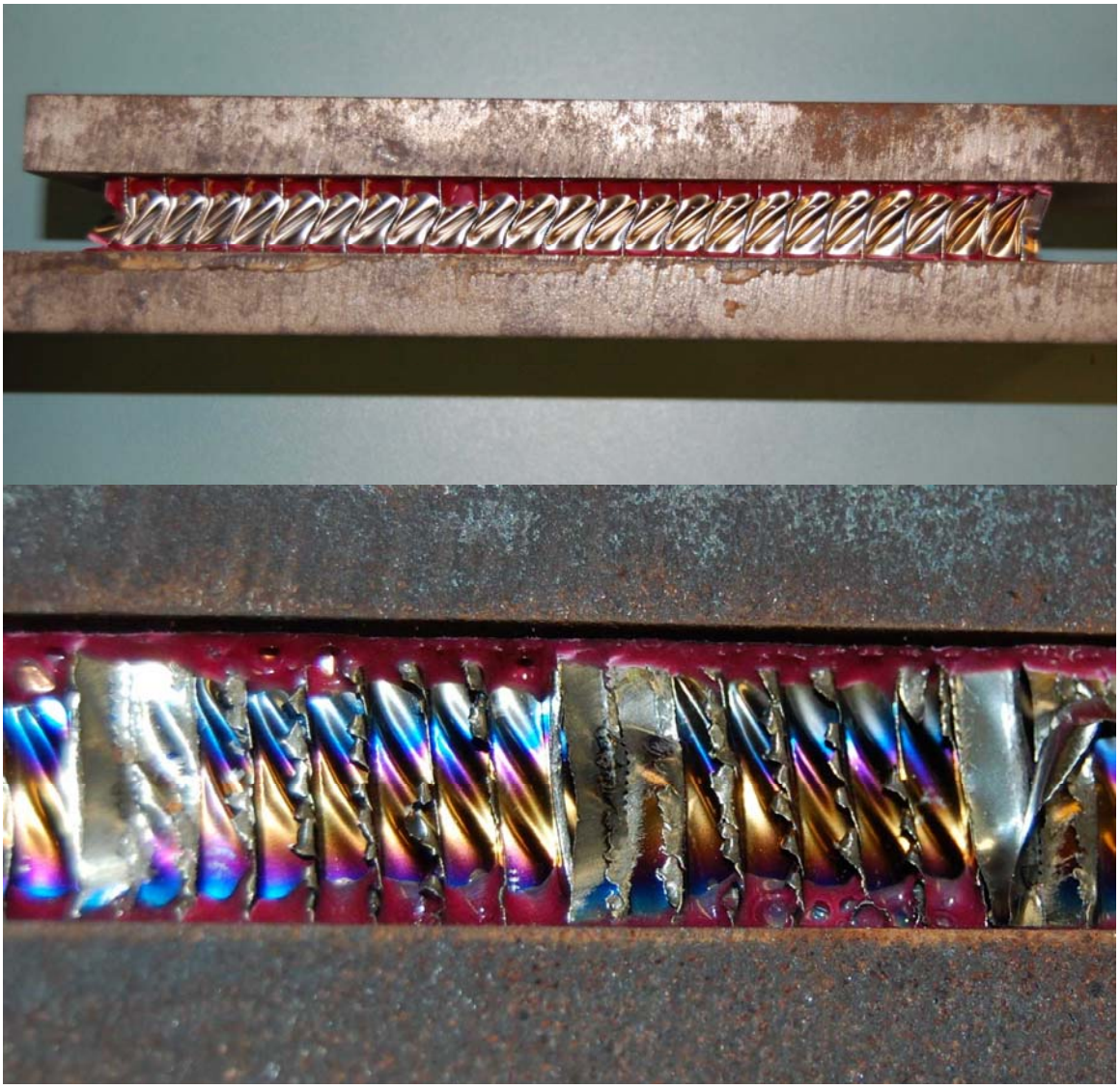

Figure E.1: Images of shear bands in two different shear specimens

Appendix F

Exerpts from SAS Output Results for Shear Properties

Model Information

Data Set	WORK.SHEAR
Dependent Variable	**US (shear strength)**
Covariance Structure	Variance Components
Estimation Method	REML
Residual Variance Method	Profile
Fixed Effects SE Method	Model-Based
Degrees of Freedom Method	Satterthwaite

Class Level Information

Class	Levels	Values
FT	2	0.001 0.0015
CS	2	0.108 0.125
CH	3	1 2 3
O	3	SA SR SX
B	5	1 2 3 4 5
S	6	1 2 3 4 5 6

Dimensions

Covariance Parameters	3
Columns in X	144
Columns in Z	200
Subjects	1
Max Obs Per Subject	1080

Number of Observations

Number of Observations Read	1080
Number of Observations Used	1080
Number of Observations Not Used	0

Type 3 Tests of Fixed Effects

Effect	Num DF	Den DF	F Value	Pr > F	
FT	1	16	1427.20	<.0001	*
CS	1	16	127.74	<.0001	*
FT*CS	1	16	8.88	0.0088	*
CH	2	128	321.43	<.0001	*
FT*CH	2	128	23.37	<.0001	*
CS*CH	2	128	1.08	0.3429	
FT*CS*CH	2	128	4.00	0.0206	*
O	2	128	276.52	<.0001	*
FT*O	2	128	48.70	<.0001	*
CS*O	2	128	1.25	0.2894	
FT*CS*O	2	128	0.77	0.4654	
CH*O	4	128	5.86	0.0002	*
FT*CH*O	4	128	1.37	0.2467	
CS*CH*O	4	128	0.08	0.9889	
FT*CS*CH*O	4	128	1.22	0.3044	

Model Information

Data Set	WORK.SHEAR
Dependent Variable	**Mod (shear modulus)**
Covariance Structure	Variance Components
Estimation Method	REML
Residual Variance Method	Profile
Fixed Effects SE Method	Model-Based
Degrees of Freedom Method	Satterthwaite

Class Level Information

Class	Levels	Values
FT	2	0.001 0.0015
CS	2	0.108 0.125
CH	3	1 2 3
O	3	SA SR SX
B	5	1 2 3 4 5
S	6	1 2 3 4 5 6

Dimensions

Covariance Parameters	3
Columns in X	144
Columns in Z	200
Subjects	1

Max Obs Per Subject	1080

Number of Observations

Number of Observations Read	1080
Number of Observations Used	1080
Number of Observations Not Used	0

Type 3 Tests of Fixed Effects

Effect	Num DF	Den DF	F Value	Pr > F	
FT	**1**	**16**	**1121.88**	**<.0001**	*****
CS	**1**	**16**	**248.40**	**<.0001**	*****
FT*CS	**1**	**16**	**32.17**	**<.0001**	*****
CH	**2**	**128**	**105.80**	**<.0001**	*****
FT*CH	**2**	**128**	**91.00**	**<.0001**	*****
CS*CH	**2**	**128**	**22.26**	**<.0001**	*****
FT*CS*CH	**2**	**128**	**2.31**	**0.1029**	
O	**2**	**128**	**83.22**	**<.0001**	*****
FT*O	**2**	**128**	**2.93**	**0.0569**	******
CS*O	**2**	**128**	**0.06**	**0.9437**	
FT*CS*O	**2**	**128**	**3.00**	**0.0533**	******
CH*O	**4**	**128**	**4.68**	**0.0015**	*****
FT*CH*O	**4**	**128**	**2.03**	**0.0946**	******
CS*CH*O	**4**	**128**	**0.63**	**0.6424**	
FT*CS*CH*O	**4**	**128**	**4.18**	**0.0032**	*****